Scanning TEM (STEM) part II

Duncan Alexander
EPFL-IPHYS-LSME

STEM II contents

- Reciprocity theorem and phase contrast BF STEM
- Incoherence in STEM imaging
- STEM focusing and electron Ronchigram (lens with C_S)
- C_S-aberration correction in STEM
- HAADF theory and simulation
- Phase contrast STEM for light atoms (ABF, iCOM/iDPC, electron ptychography)

Reciprocity Theorem

Reciprocity Theorem (from geometric optics): The amplitude of a wave at detector B due to an electron source at A (STEM) is equal to the amplitude at image place A' due to a source at B' (CTEM).

⟹ Optical equivalence of CTEM vs STEM imaging

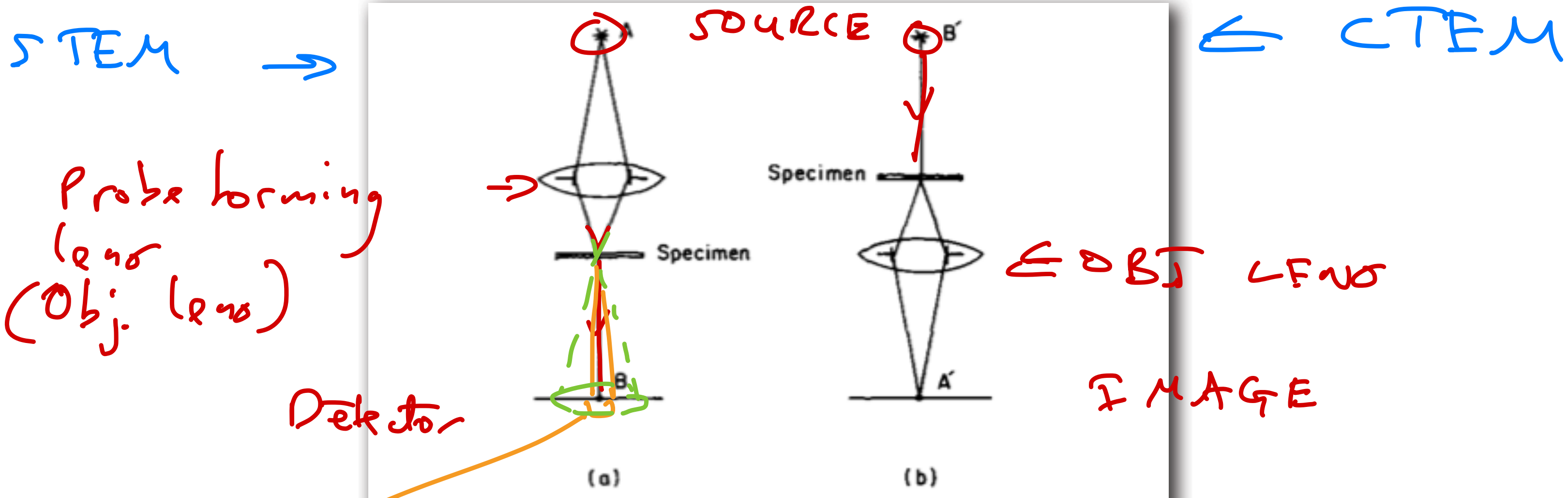

Fig. 1. The essential elements of the electron-optical systems for (a) the transmission scanning electron microscope, (b) the conventional transmission electron microscope.

J.M. Cowley *Applied Physics Letters* **15** (1969) 58

Very small detector!
⇒ Inefficient

Quiz: for reciprocity with BF CTEM with a perfectly parallel incident beam, what collection angle do we need for the BF detector in STEM?

Phase contrast BF STEM imaging

- Following from the theory of reciprocity, with a sufficiently small probe a BF detector can produce an image equivalent to a HR-TEM image.
- This is conditional on having CBED discs overlapping on the BF detector.
- No overlap is like BF CTEM imaging with only the direct beam chosen, so will give no fringes

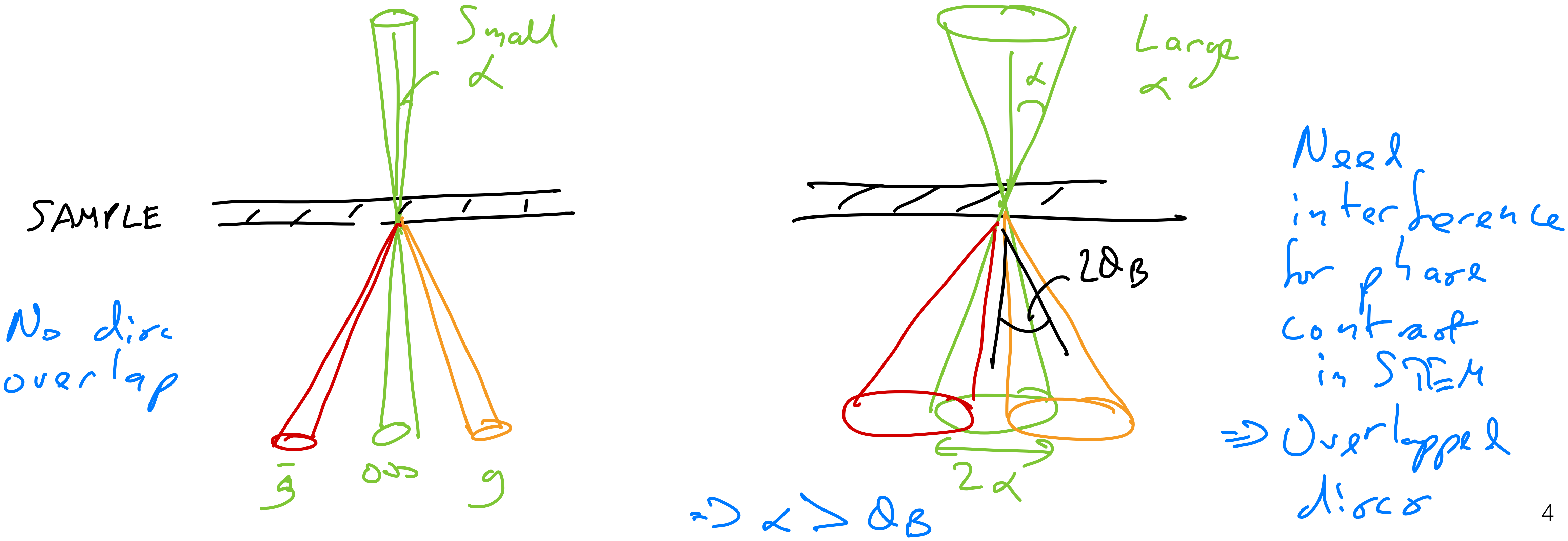

Phase contrast BF STEM imaging

- Following from the theory of reciprocity, with a sufficiently small probe a BF detector can produce an image equivalent to a HR-TEM image.
- This is conditional on having CBED discs overlapping on the BF detector.
- No overlap is like BF CTEM imaging with only the direct beam chosen, so will give no fringes

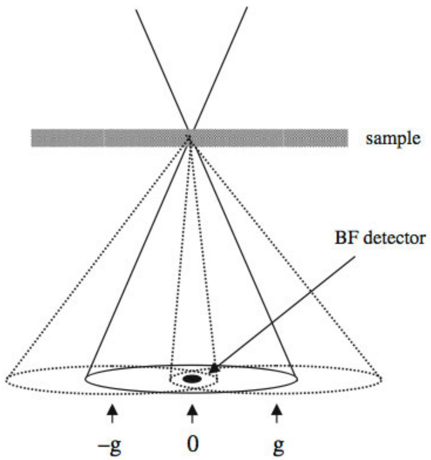

Figure 2–3. Diffraction of the coherent convergent beam by a specimen leads to diffracted discs. Where these discs overlap, interference will be seen. The bright-field detector is sensitive to interference between the direct beam and the two opposite diffracted beams.

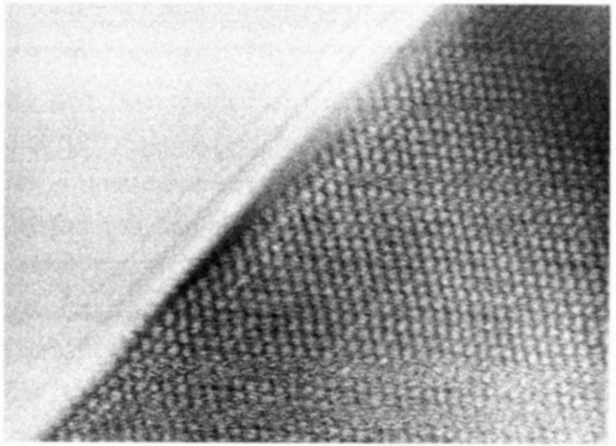

Figure 3. Bright-field STEM image of a small MgO crystal in [1 1 0] orientation [95].

Phase contrast STEM

Quiz: for a particular lattice spacing, how can we increase disc overlap in the diffraction pattern?

e.g. increase C2 aperture size

Coherent elastic scattering

Incoherence in STEM imaging

Coherent vs Incoherent imaging

- HR bright-field STEM image of a weak phase object has following intensity equation:

$$I_{\mathrm{BF}}(\boldsymbol{R}) = \left|\varphi(\boldsymbol{R}) \otimes P(\boldsymbol{R})\right|^2$$

  where $\boldsymbol{R}$ is a 2D position vector, $\varphi(\boldsymbol{R})$ is a phase shift and $P(\boldsymbol{R})$ is the probe amplitude distribution

- Therefore can show positive or negative contrast depending on the phase of the transfer function

- If instead integrate *all* beams scattered onto an annular dark-field detector, obtain:

$$I(\boldsymbol{R}_0) = \left|\varphi(\boldsymbol{R}_0)\right|^2 \otimes \left|P(\boldsymbol{R}_0)\right|^2$$

  where $\boldsymbol{R}_0$ is a scan coordinate that locates centre of the e^- probe

- This is a *convolution of intensities*

Coherent vs Incoherent imaging

- A convolution of intensities corresponds to an *incoherent* imaging condition

- Compared to coherent – i.e. phase contrast – imaging, incoherent imaging has some specific (useful!) characteristics:

  ➡ No image contrast inversion with defocus

  ➡ “Camera-like characteristics”

  ➡ Broad optical transfer function (OTF) instead of modulating PCTF

  ➡ Improved point resolution for same optical characteristics

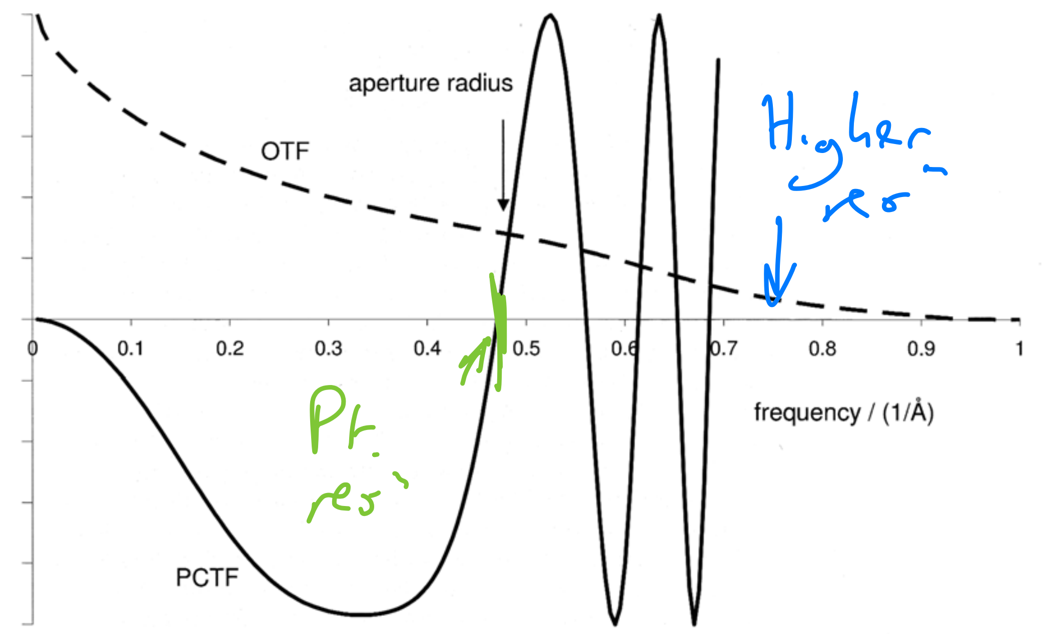

Figure 2–12. A comparison of the incoherent object transfer function (OTF) and the coherent phase-contrast transfer function (PCTF) for identical imaging conditions (V = 300 kV, C_S = 1 mm, z = −40 nm).

Resolution of incoherent imaging

- The above result means that an ADF STEM image has an improved spatial resolution (point resolution) compared to its BF counterpart
- Theory was originally developed by biologists
- However, strong diffraction from crystalline samples ⟹ lower-angle ADF detector collects too much coherent diffraction signal to achieve such incoherency
- HAADF detector does achieve incoherent imaging criterion because uses *phonon-scattered* electrons that are fundamentally incoherent
  – i.e. the scattering mechanism destroys the phase relationship

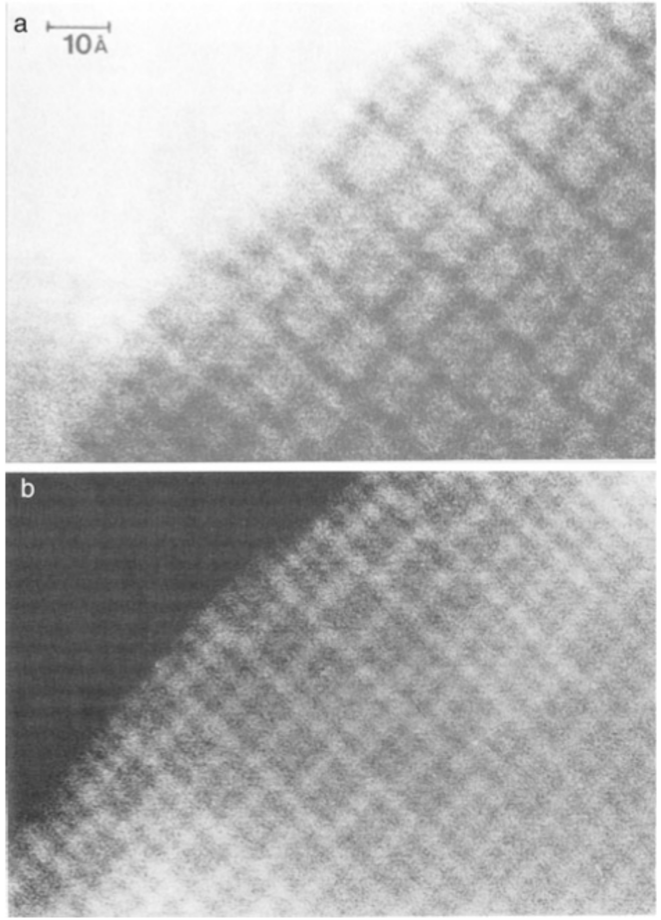

Figure 1–14. (**a**) Bright field and (**b**) ADF images of $Ti_2Nb_{10}O_{29}$ showing improved atomic resolution detail in the dark field image, reproduced from Cowley (1986b) with permission.

STEM focusing and the electron Ronchigram

STEM focusing

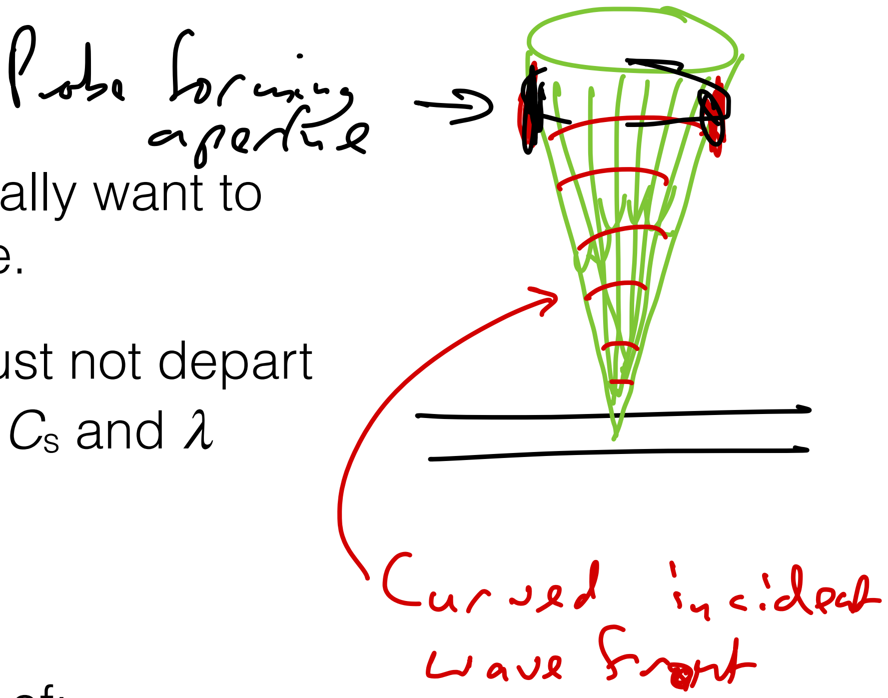

- Consider probe-forming (objective) lens with C_s. Ideally want to form e– probe from rays which have the same phase.

- Approximate using criterion that phase shift $\chi(\vec{q})$ must not depart more than $\pi/4$ from 0. It is the found that for a given C_s and λ optimal defocus is:

$$z = -0.71\lambda^{1/2} C_s^{1/2}$$

- Condition allows probe-forming aperture with radius of:

$$\alpha = 1.3\lambda^{1/4} C_s^{-1/4}$$

Talos: λ 2.5 pm, C_s 1.2 mm $\rightarrow \alpha \approx 9$ mrad

- Using this optimum defocus and aperture size, the probe FWHM is given by:

$$d = 0.4\lambda^{3/4} C_s^{1/4}$$

Talos: $d \sim 1.5$ Å

(HRTEM pt. res.: $d = 0.66\lambda^{3/4} C_s^{1/4}$)

"Scanning Transmission Electron Microscopy", P.D. Nellist, in *Science of Microscopy Vol. 1*, Springer 2007

The electron Ronchigram

- STEM mode; fix the probe; large/no aperture in probe-forming lens
- Record 2-D image of intensity in diffraction (i.e. STEM detector) plane
- See “shadow image” of sample in the direct beam diffraction disc

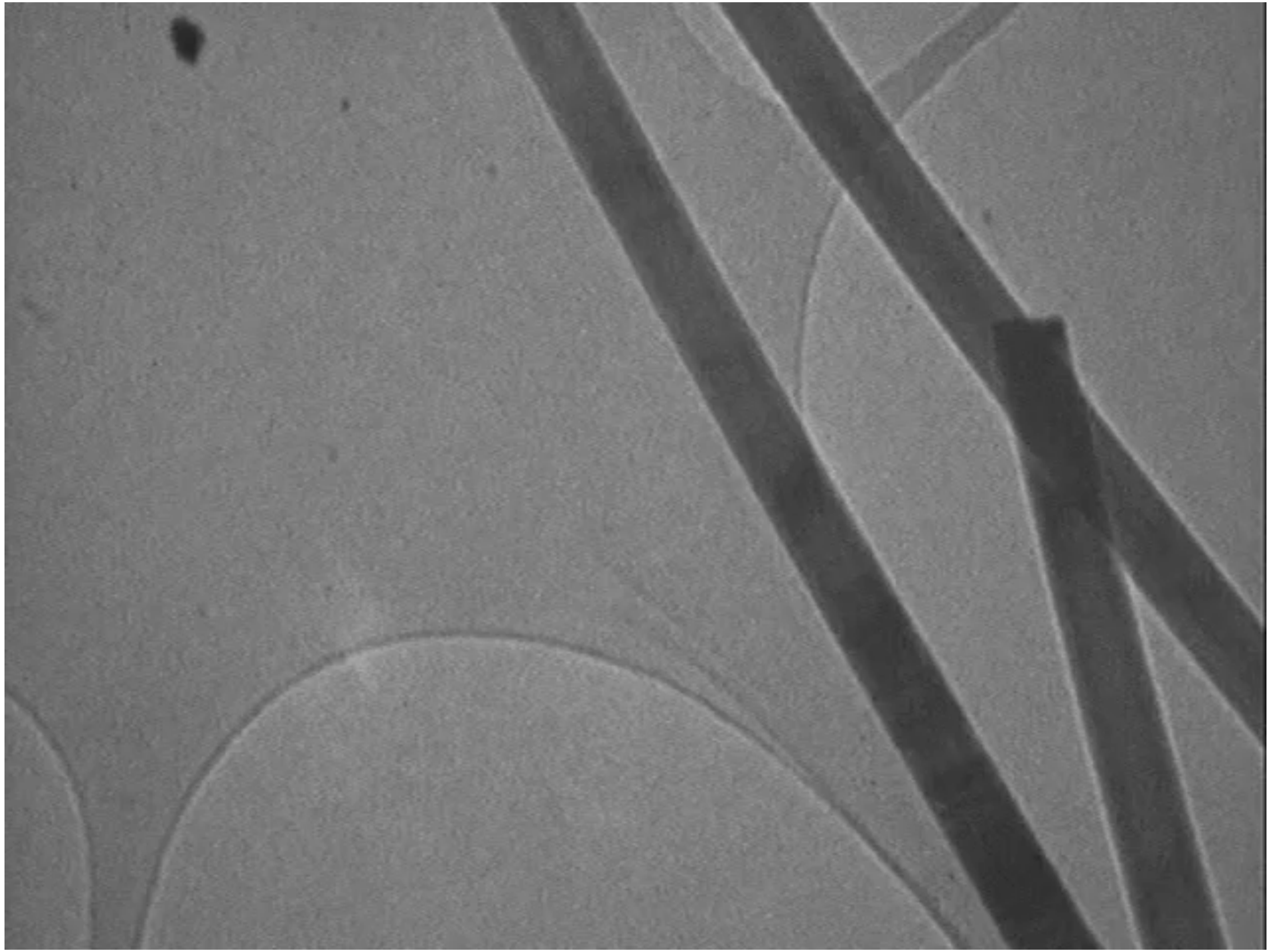

Basics of shadow image formation

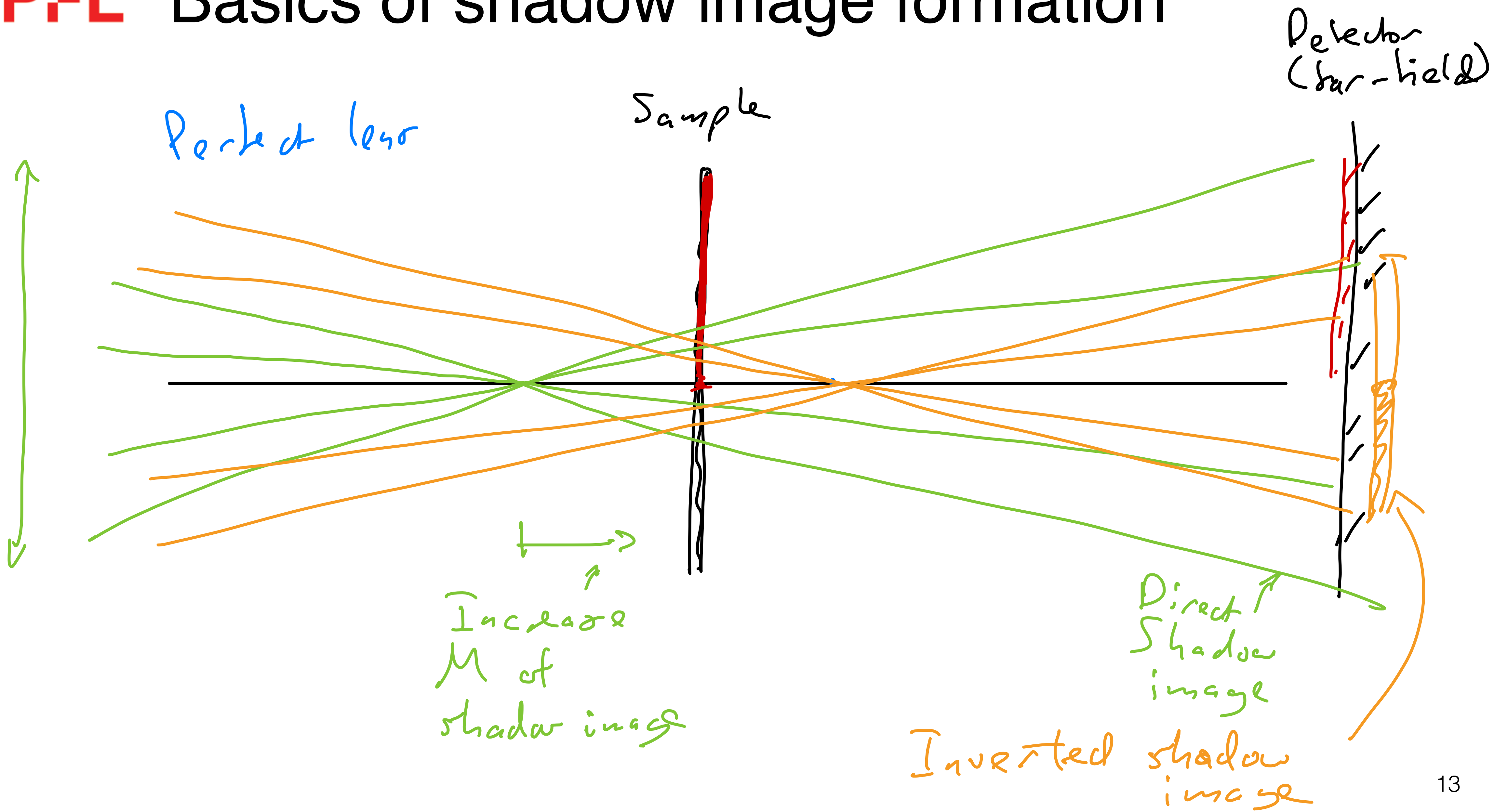

Basics of shadow image formation

- Assuming perfect optics:

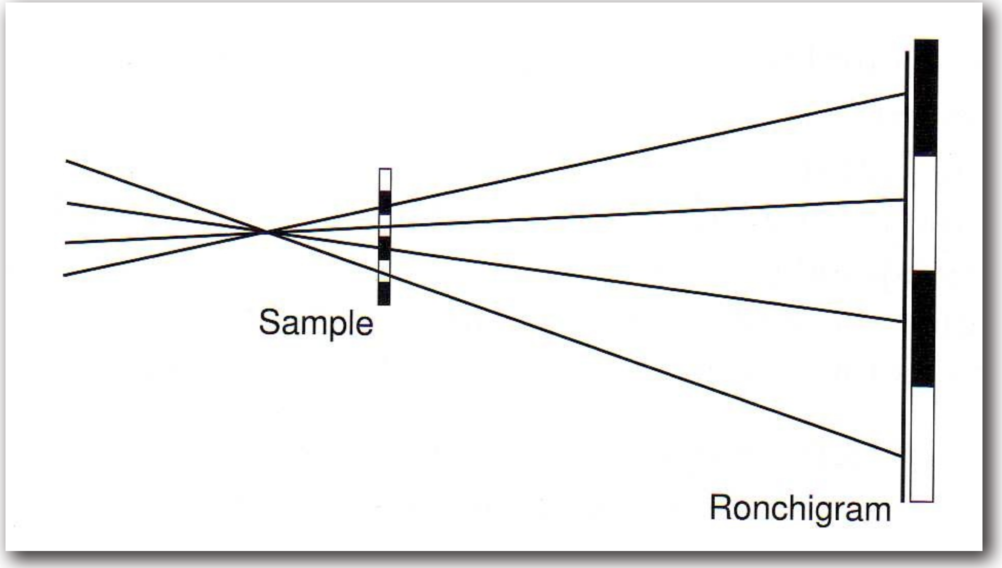

- Ronchigram is similar to defocused TEM diffraction pattern, blending image information with scattering angles
- At overfocus the STEM detector plane is a shadow image of the sample magnification $M = d_{\text{probe–detector}} / d_{\text{probe–sample}}$
- At underfocus the image will be magnified, but also inverted

Diagram from: "Scanning Transmission Electron Microscopy", P.D. Nellist, in *Science of Microscopy Vol. 1*, Springer 2007

Shadow image formation with C_s

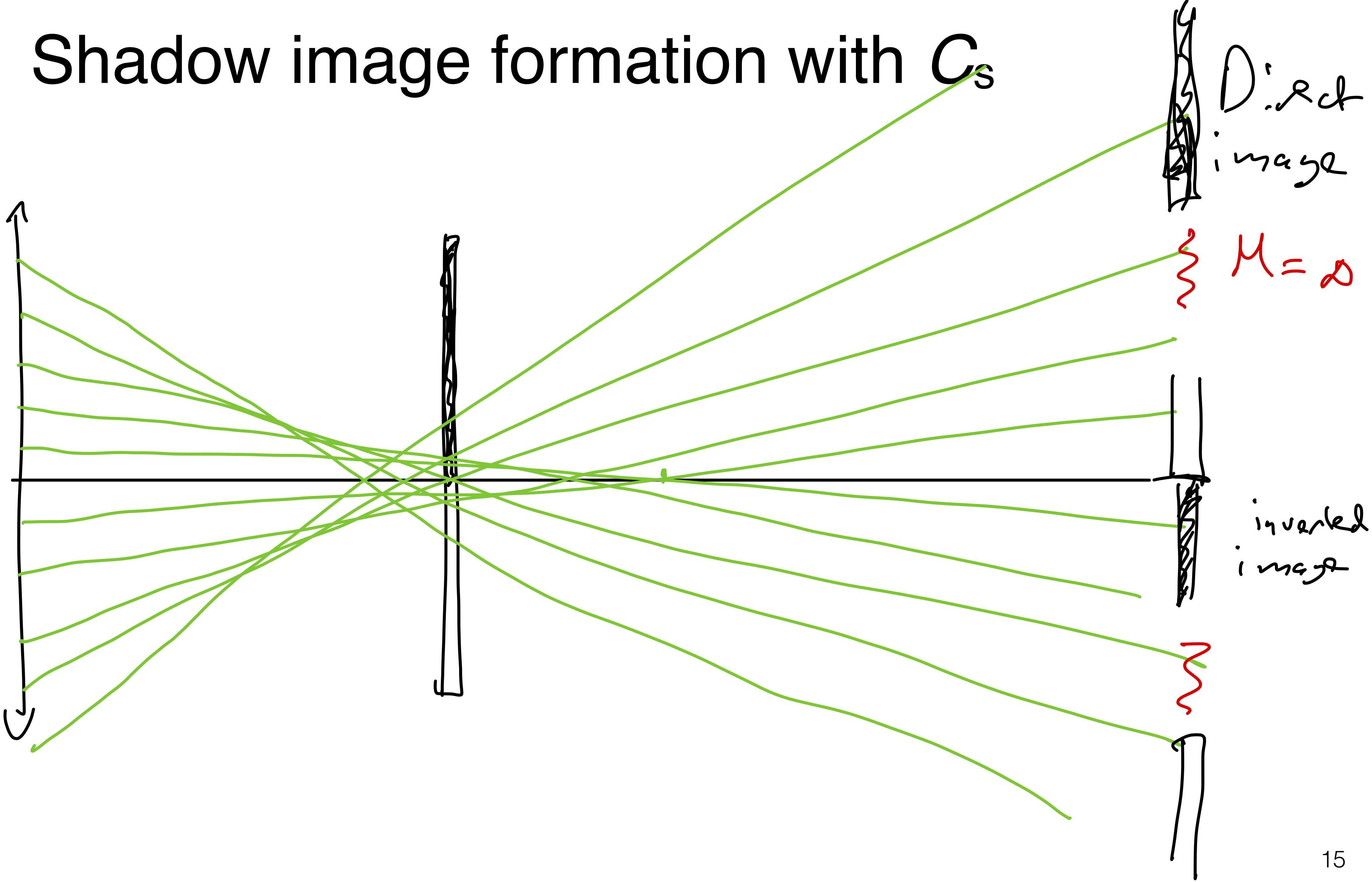

Shadow image formation with C_S

- For lens with positive C_S, focal point of rays depends on their angle

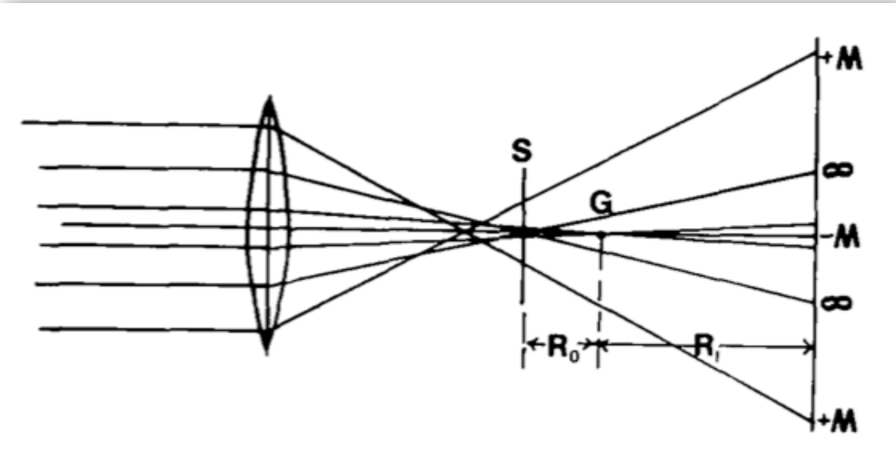

- Consider sample *S* in underfocus for paraxial rays:
- Paraxial rays with Gaussian focus *G* have magnification $M = -R_1/R_0$
- Rays that cross at *S* have infinite magnification
- Ronchigram focal series:

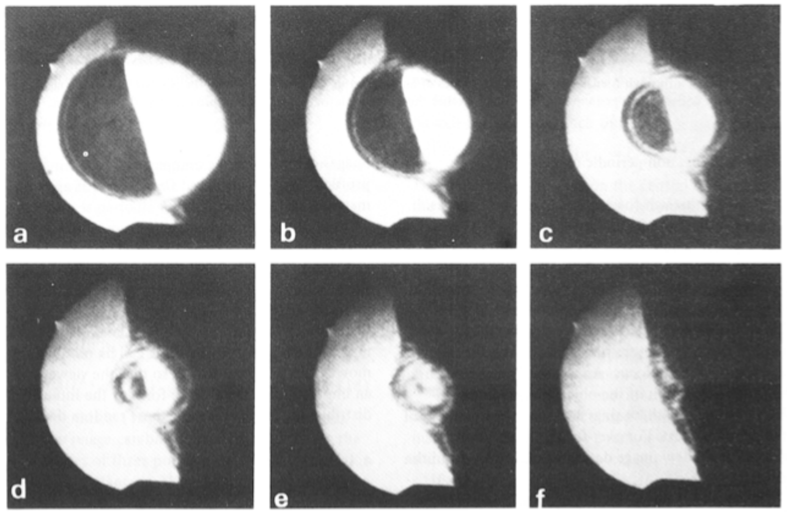

Fig. 3. Through-focus series of shadow images of the edge of a thick crystal. An asymmetry of the scanning in the display system gives the infinite-magnification circles a slightly elliptical shape. Approximate defocus values: (a) −1.2 μm, (b) −0.7 μm, (c) −0.5 μm, (d) −0.25 μm, (e) 0 μm, (f) +0.25 μm.

- When sample at Gaussian focal point or in overfocus for paraxial rays: direct image of sample, with magnification decreasing smoothly for larger angles

Figures from J.M. Cowley *Ultramicroscopy* **4** (1979) 435

Radii & azimuths of infinite magnification

Sample: amorphous carbon

- The under focus Ronchigram shows infinite magnification at more than one scattering angle
- There are radii (radial spokes) and tangential azimuths (rings) of infinite magnification
- Why is this?

Direct shadow image

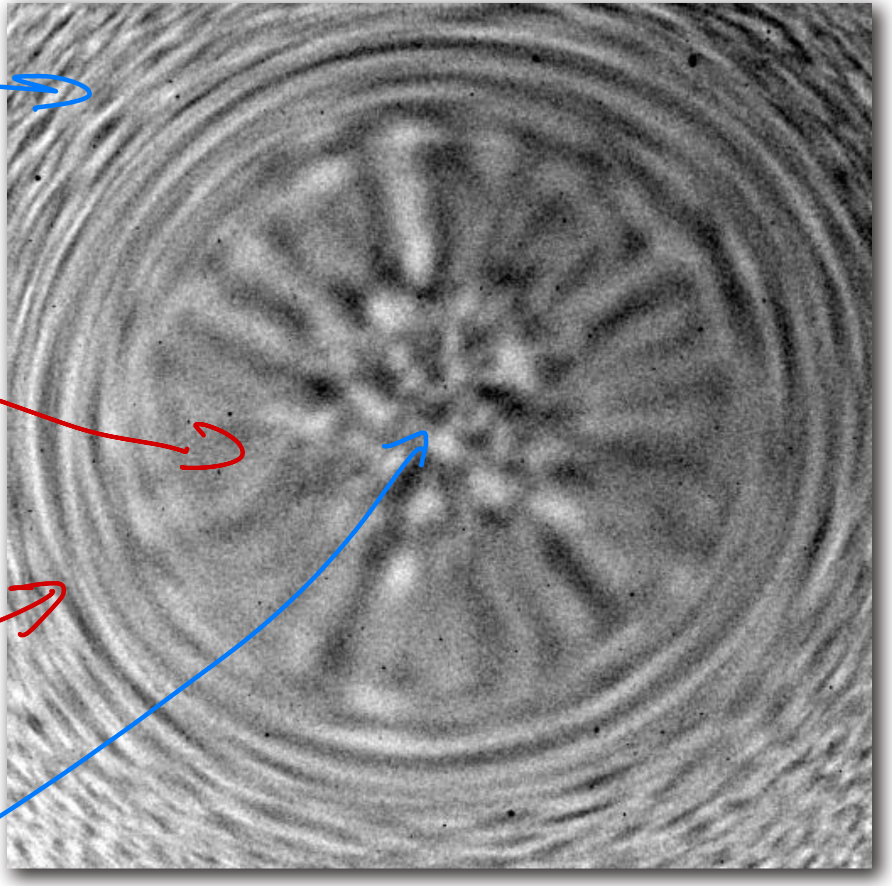

Inverted shadow image

Radii & azimuths of infinite magnification

- Phase shift due to aberration in *Front Focal Plane* of objective (probe-forming) lens:

  $\chi(\vec{q}) = \left(\pi z \lambda |\vec{q}|^2 + \frac{1}{2}\pi C_s \lambda^3 |\vec{q}|^4\right)$ for defocus z and wave vector $\vec{q}$ where $|\vec{q}| = \theta/\lambda$

- Cowley derived that, in a 1-D optical system: $M' = \dfrac{M}{1 + C_s \lambda^2 |\vec{q}|^2 / z}$ ← Defocus

  M: magnification for ideal $C_s = 0$; M' :actual magnification

- Infinite magnification at: $|\vec{q}|^2 = \dfrac{-z}{C_s \lambda^2}$

- In a 2-D optical system there are **two** critical angles:
  - ➡ Radial magnification is infinite for: $|\vec{q}|^2 = \dfrac{-z}{3 C_s \lambda^2}$ ← z: defocus
  - ➡ Circumferential magnification is infinite for: $|\vec{q}|^2 = \dfrac{-z}{C_s \lambda^2}$

J.M. Cowley *Journal of Electron Microscopy Technique* **3** (1986) 25

Aligning STEM mode

- The Ronchigram of amorphous carbon is to STEM as the FFT of amorphous carbon is to CTEM: use it to correct objective lens astigmatism and tune defocus

- Example: tuning astigmatism:

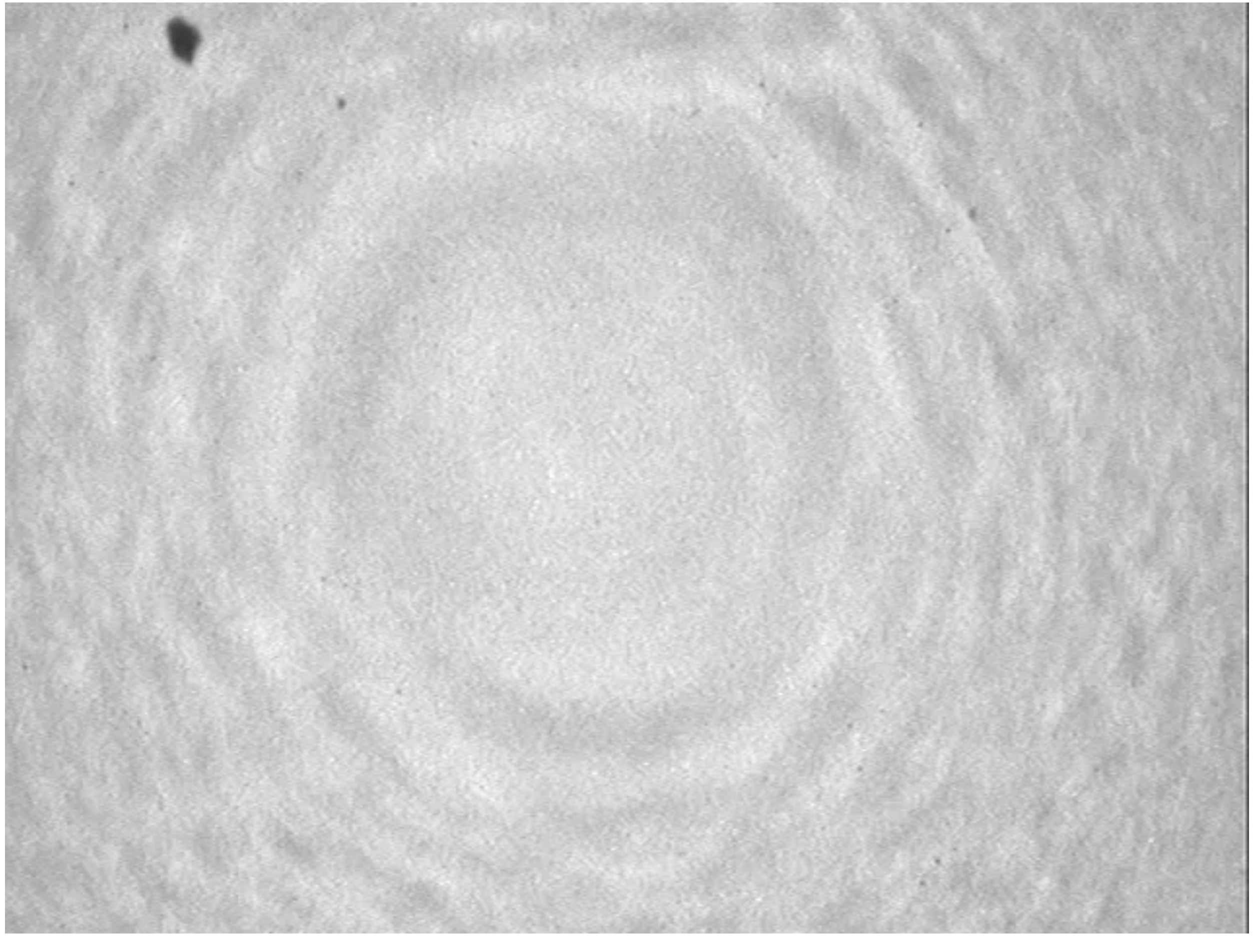

Aligning STEM mode

- The Ronchigram of amorphous carbon is to STEM as the FFT of amorphous carbon is to CTEM: use it to correct objective lens astigmatism and tune defocus
- Focusing with Ronchigram:
  - Reduce under-focus until infinite-magnification rings are of minimum diameter $\Longrightarrow$ optimum defocus (c.f. Scherzer defocus in HR-TEM)

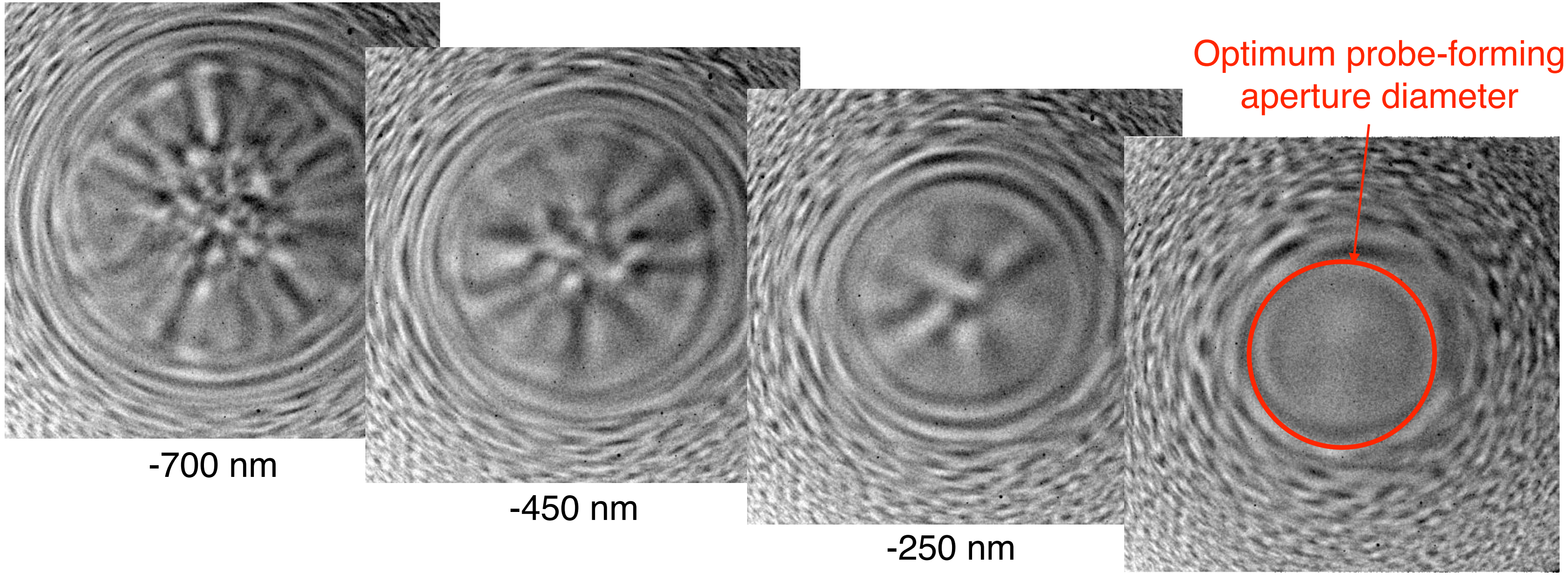

  - Fit probe-forming aperture to the “sweet spot” or “blow up” region of constant phase within this diameter

C_S-aberration correction in STEM

C_S-aberration correction in STEM

- Correcting the C_S of the probe-forming lens overcomes above limits
- Correction realised by coupling radially-symmetric, convergent EM lenses with positive C_S with non-symmetric lenses which are divergent and so have negative C_S
- Pioneering STEM corrector: quadrupole–octopole design by NION (Krivanek):

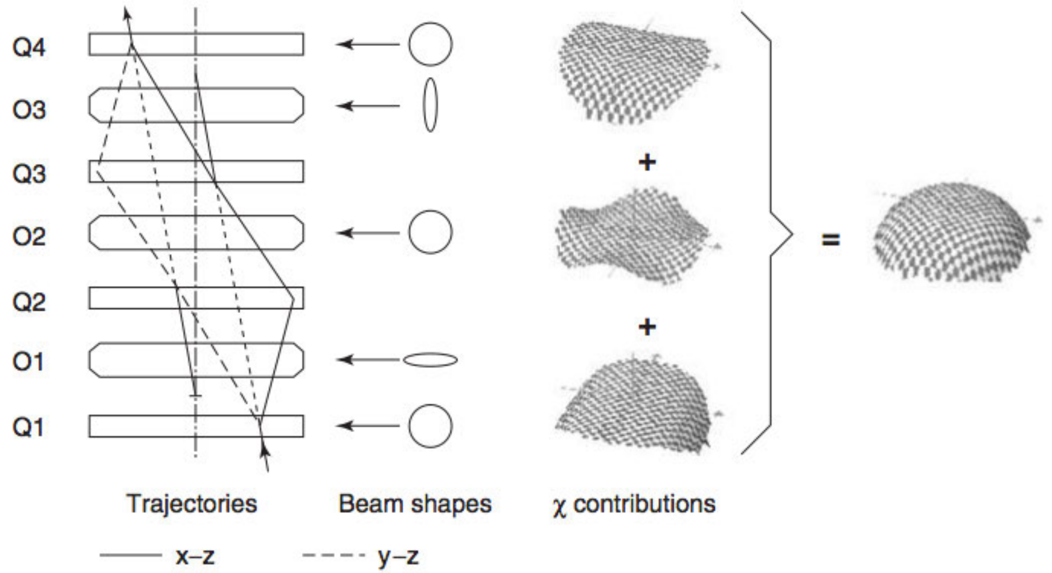

FIGURE 12.6 Trajectories and aberration function contributions in a quadrupole–octopole corrector.

Figure from Krivanek et al. Aberration Correction in Electron Microscopy, Handbook of Charged Particle Physics 2009, pp. 601–641

C_S-aberration correction in STEM

- Correcting the C_S of the probe-forming lens overcomes above limits
- Correction realised by coupling radially-symmetric, convergent EM lenses with positive C_S with non-symmetric lenses which are divergent and so have negative C_S
- Most common STEM corrector: hexapole–round lens–hexapole by CEOS:

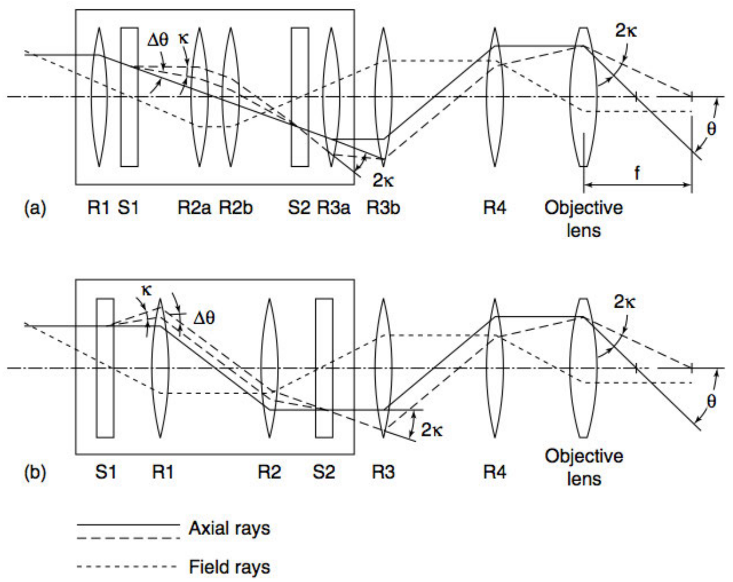

FIGURE 12.8 Sextupole—round lens—sextupole corrector designs. (Shao, Z., *Rev. Sci. Instrum.*, **59**, 2429, 1988; Rose, H., *Optik*, **85**, 19, 1990.)

DCOR version on CIME's FEI Titan Themis:
< 0.7 Å resolution at 300 kV
~1 Å resolution at 80 kV

Measuring aberrations

- With the sample at a defocus z and an incident wavefront that is not spherical local ray bundles go through cross-overs at different heights in the column
- The magnification of the shadow image becomes position-dependent, and different in different directions
- C.f. FFT of amorphous material for measuring aberrations in HR-TEM

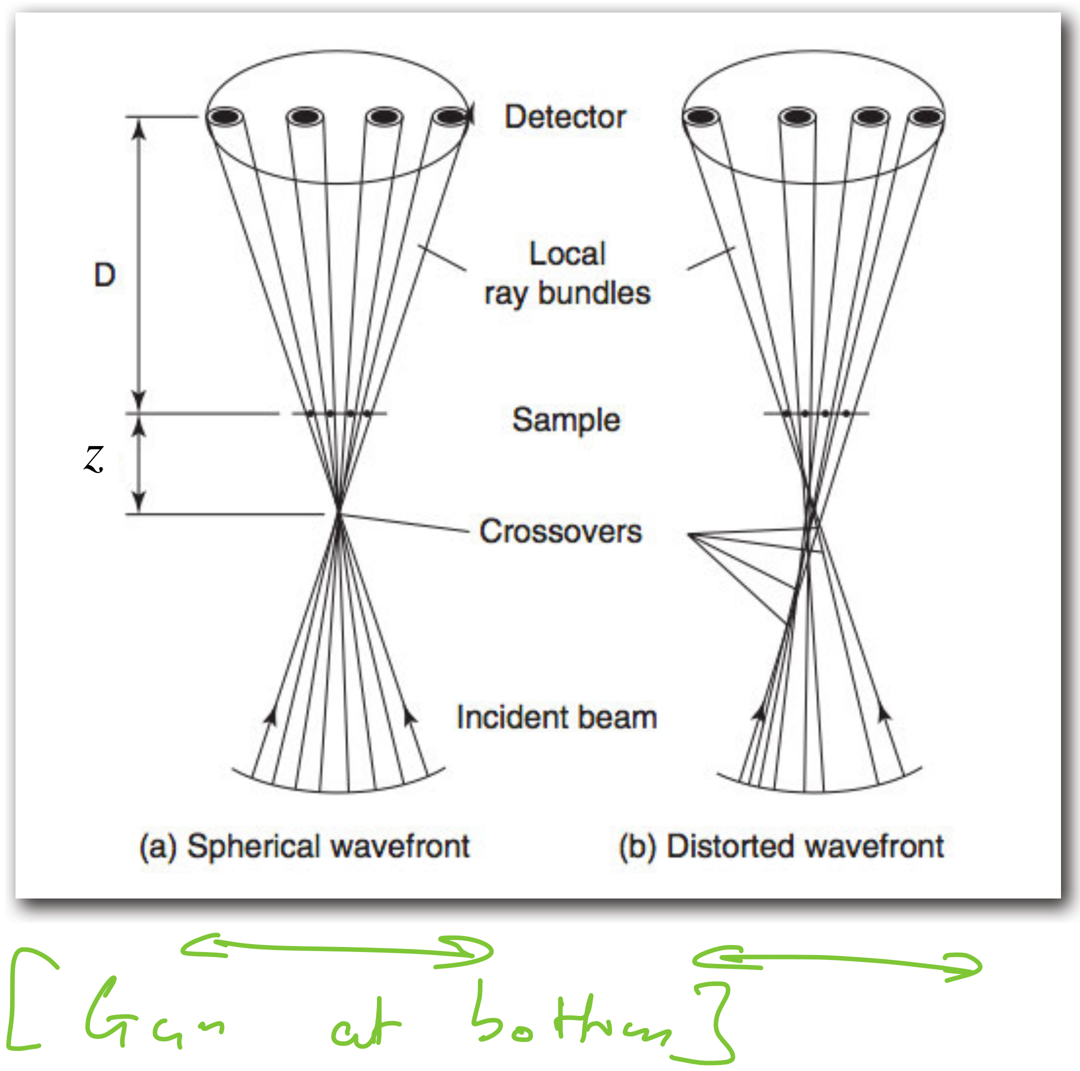

Measuring aberrations

- Quiz: which shadow image of Au nano particles on amorphous carbon film, taken at defocus of –600 nm, shows which type of aberration?
  - ➡ *Coma – i.e. incident beam tilt*
  - ➡ *Astigmatism*
  - ➡ *3-fold astigmatism*
  - ➡ *no aberration?*

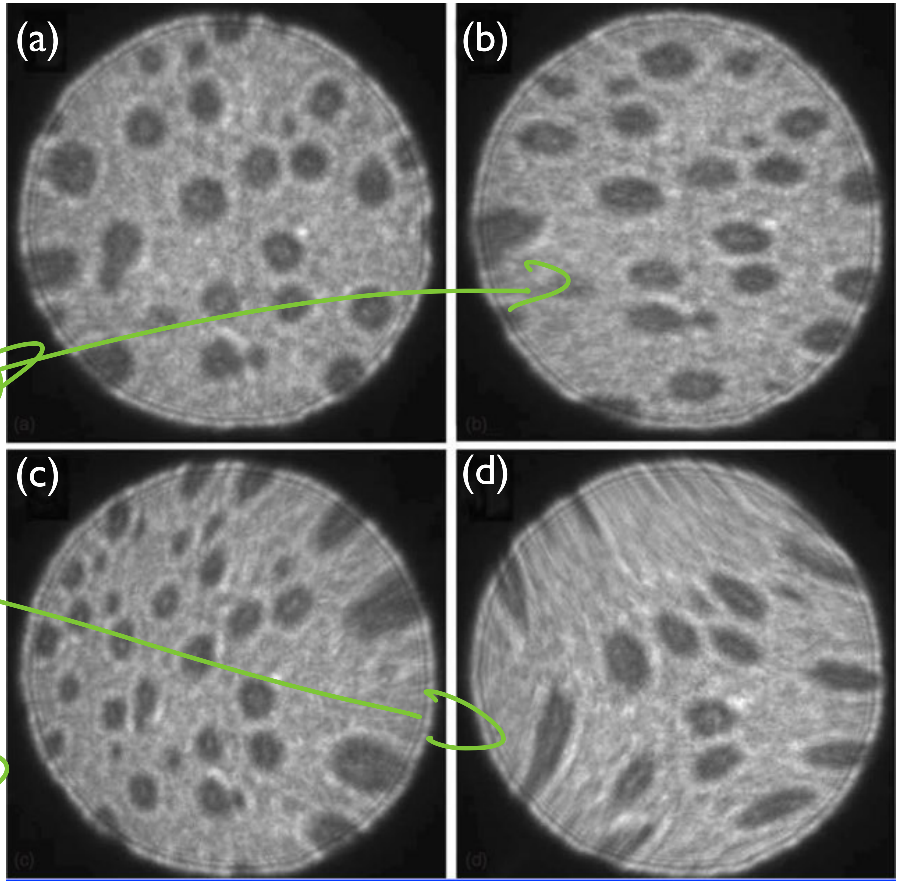

- Note: CEOS corrector alignment software instead estimates probe size and shape, by taking under-, in-, and over-focus STEM images of Au nanoparticles and performing a deconvolution. Probe shapes are measured for different incident beam tilts to measure lens aberrations.

C_s-corrected Ronchigram

- At optimum defocus aberration correction produces a sweet spot (region of flat phase) with much greater diameter

- E.g. for HT 100 kV, C_s = 1.0 mm, sweet spot has:
  With no correction $\alpha_{max} = 1.5\lambda^{1/4} C_s^{-1/4}$ = 11.6 mrad
  With C_s / C_5 correction (as shown) α_{max} = 40 mrad $\longrightarrow$

- Demagnification of virtual source size by the objective (probe-forming) lens increases in proportion with illumination angle (assuming this does not exceed sweet spot diameter) $\Longrightarrow$ Probe size decreases as $(\alpha_{max})^{-1}$

- Using larger probe-forming aperture also improves resolution slightly because diffraction limit reduced

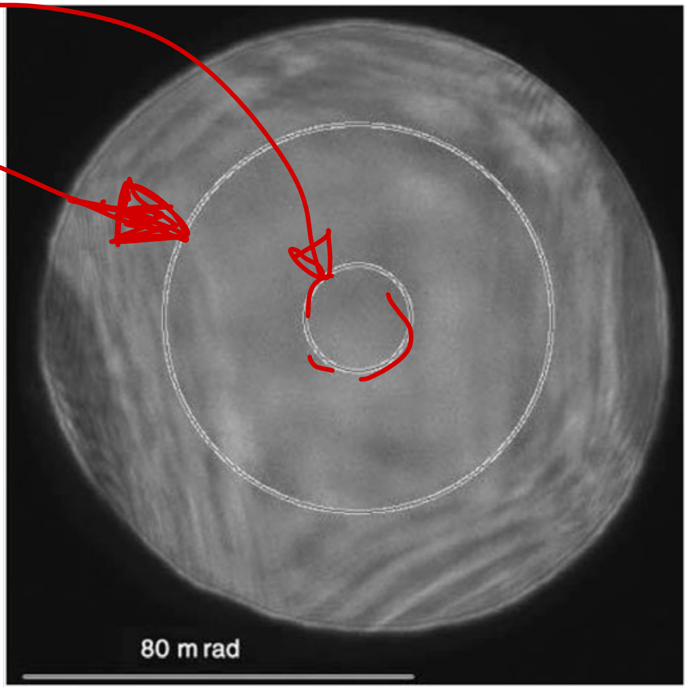

C_s-corrected Ronchigram movie

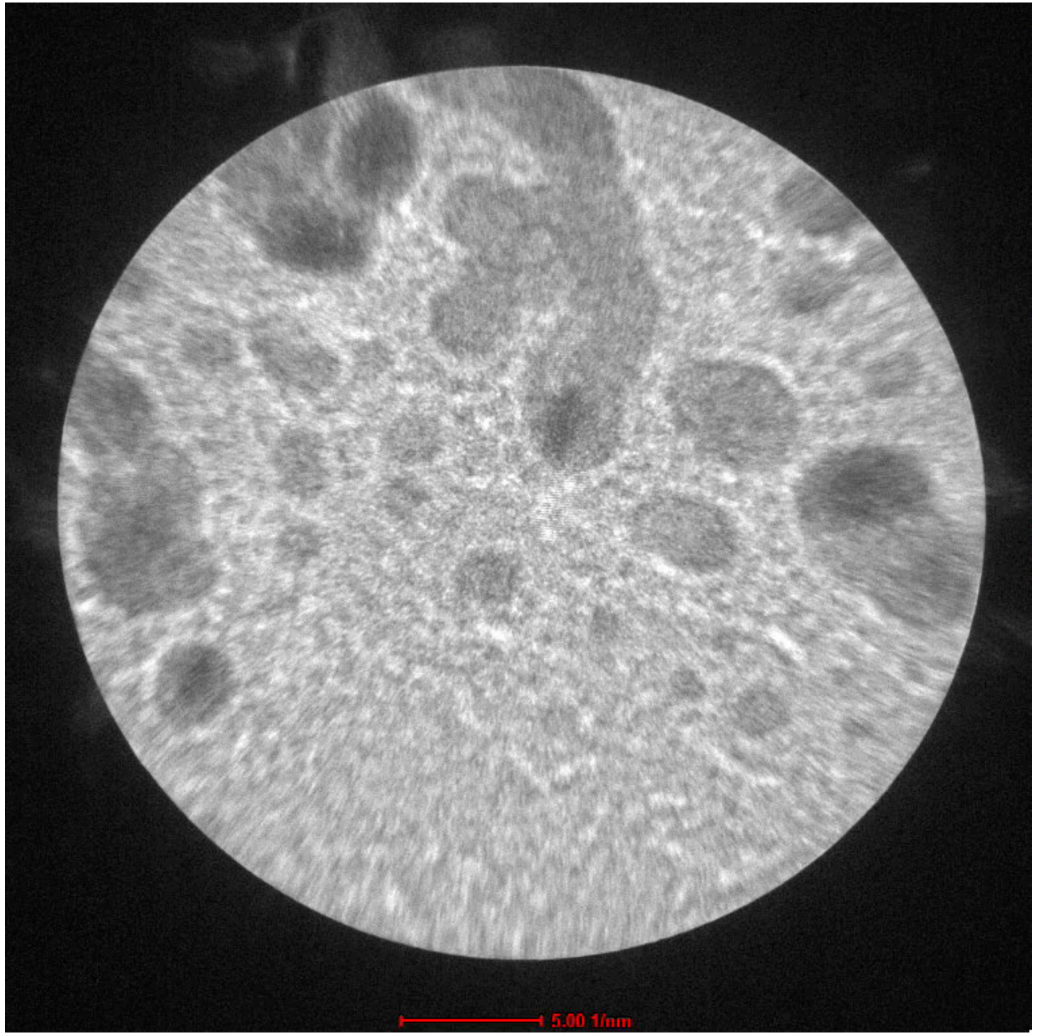

Recorded from FEI Titan Themis at CIME

C_s-corrected Ronchigram movie

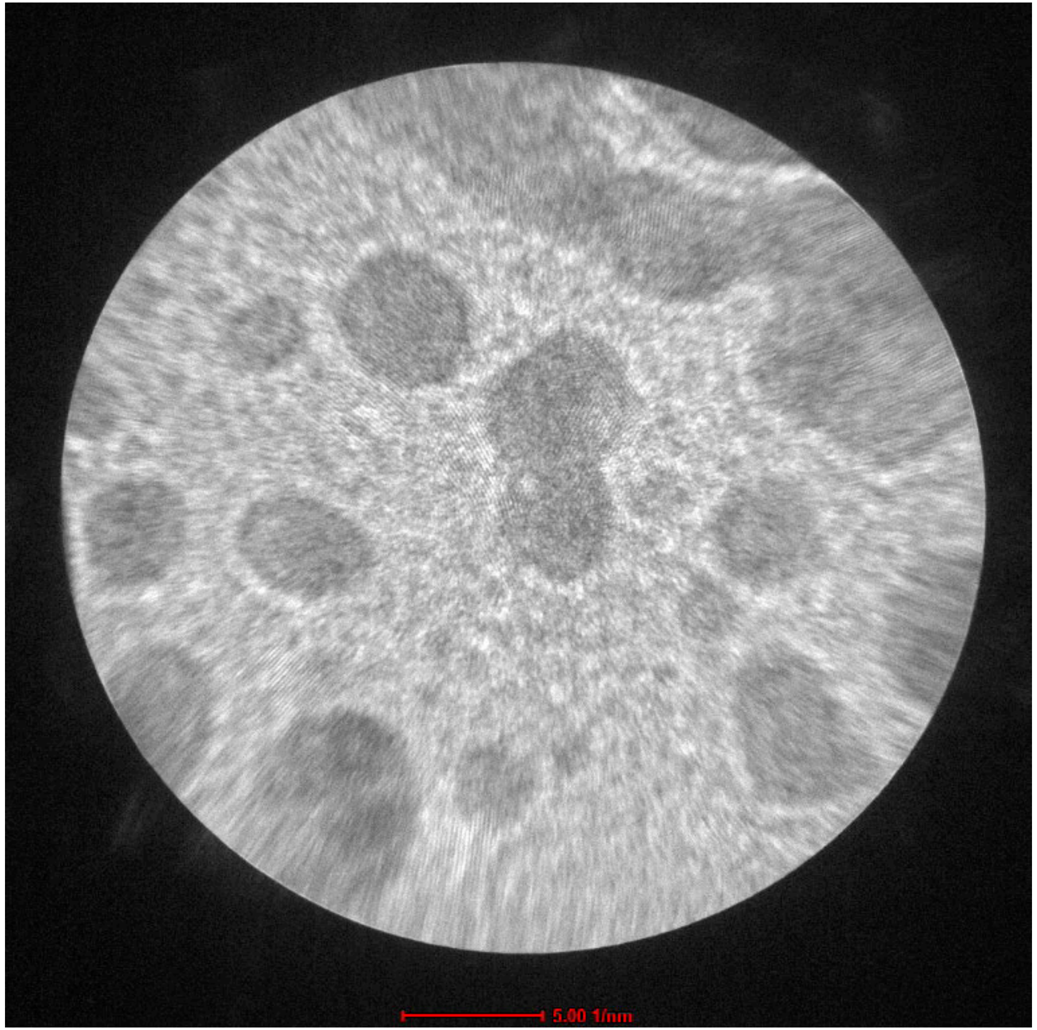

Recorded from FEI Titan Themis at CIME

Aberration-corrected examples

- Effect of C_S-correction on e^- probe intensity distribution:

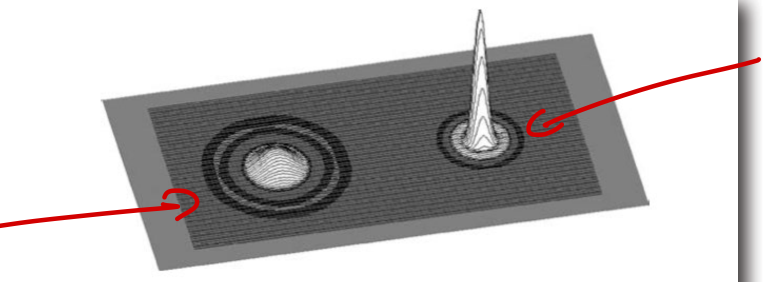

Figure 3 Calculated probe intensities before and after correction, with parameters based on the ORNL HB603U with beam energy 300 kV and energy spread 0.3 eV. (*a*) Before correction, defocus $C_1 = -63$ nm, $C_s = 1.5$ mm, $C_c = 1.3$ mm, resulting in a probe FWHM = 0.12 nm. (*b*) After correction, now $C_1 = 2$ nm, $C_s = -0.04$ mm, $C_c = 1.6$ mm and $C_5 = 100$ mm giving a probe FWHM = 0.05 nm.

Varela et al. Annu. Rev. Mater. Res. 2005 **35** 539–569

- C_S-corrected imaging example:

BF detector gives simultaneous phase contrast image equivalent to HR-TEM image; O columns visible but similar problems to interpret as HR-TEM image

Z-contrast image: "direct" interpretation, but light O columns not visible.

HAADF

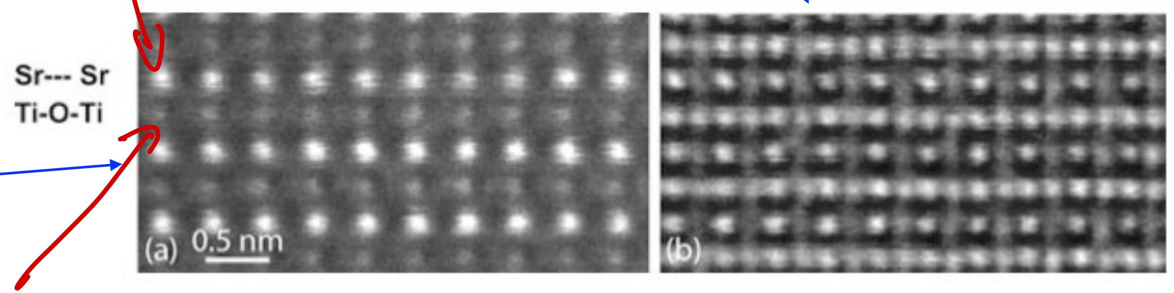

Figure 1–41. (a) Z-contrast and (b) phase contrast images of ⟨110⟩ $SrTiO_3$ taken with a VG Microscopes HB603U with Nion aberration corrector operating at 300 kV, using a defocus of +2 and +6 nm, respectively (raw data). Reproduced

Pennycook "Scanning Transmission Electron Microscopy" Chapter 1

Aberration-corrected examples – HAADF

- $(Al_xGa_{1-x})As$ nanowire

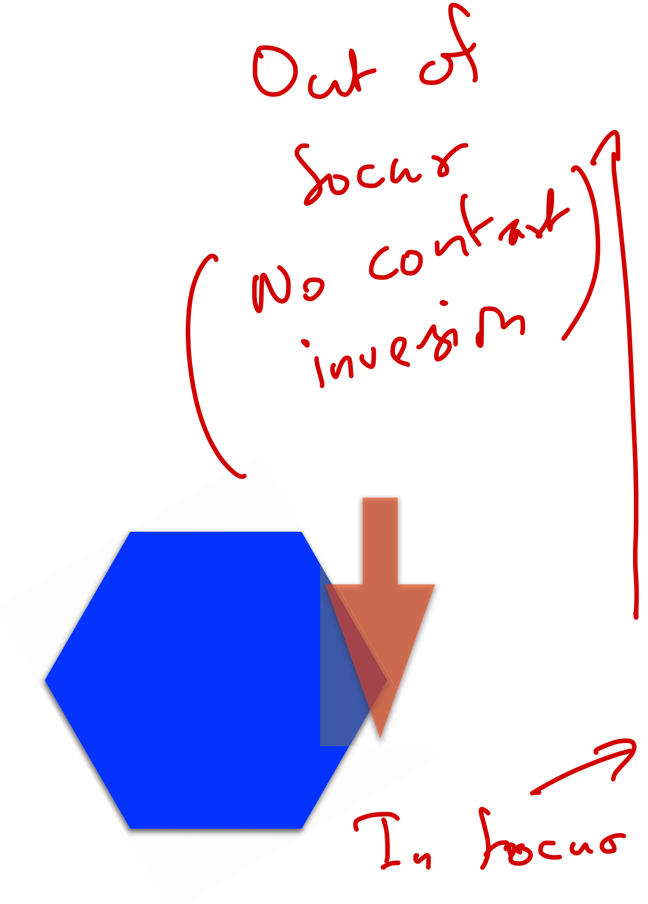

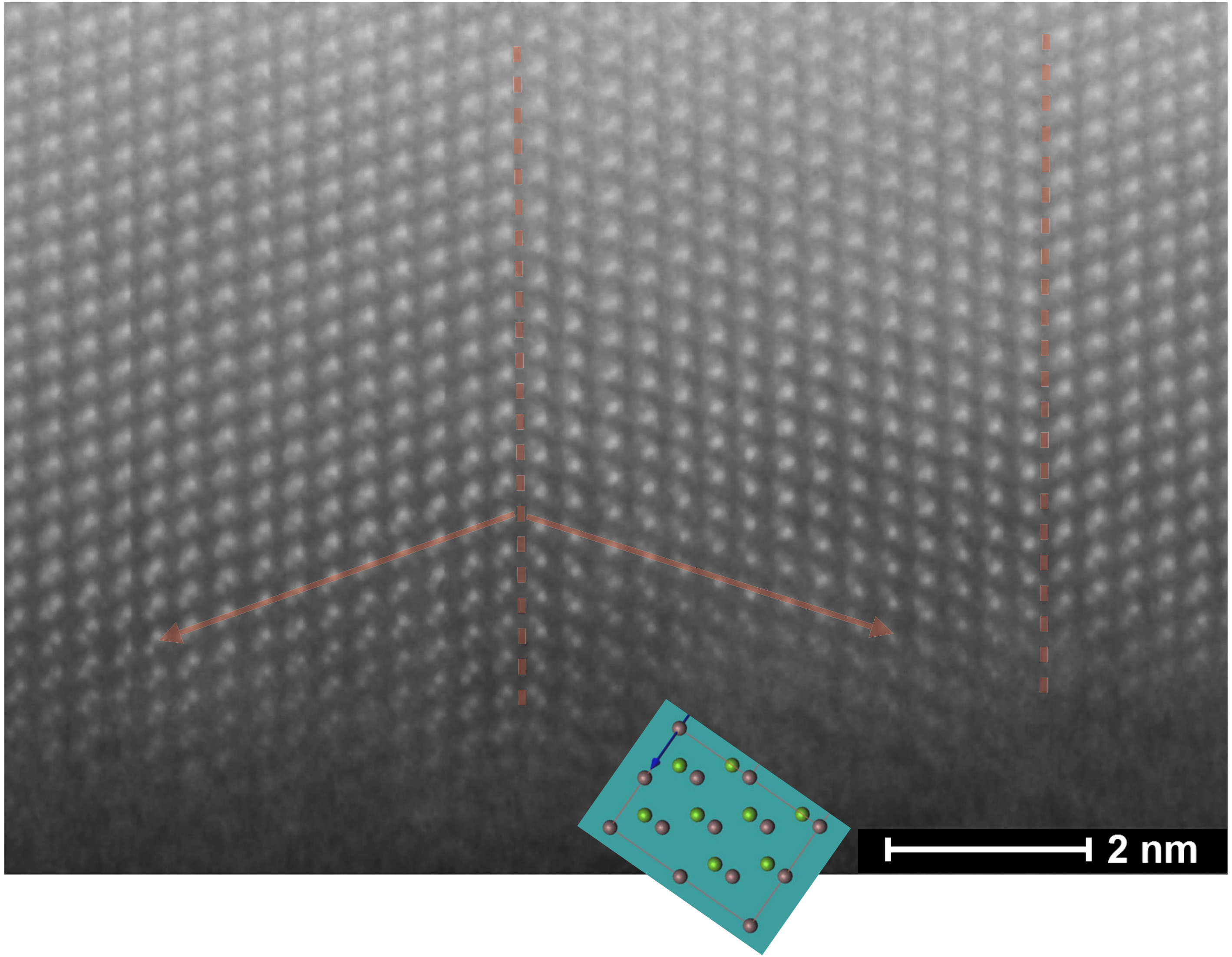

Sample courtesy of Yannick Fontana, Anna Fontcuberta-i-Morral, LMSC

Aberration-corrected examples – HAADF

- $(Al_xGa_{1-x})As$ nanowire

Zinc blende →

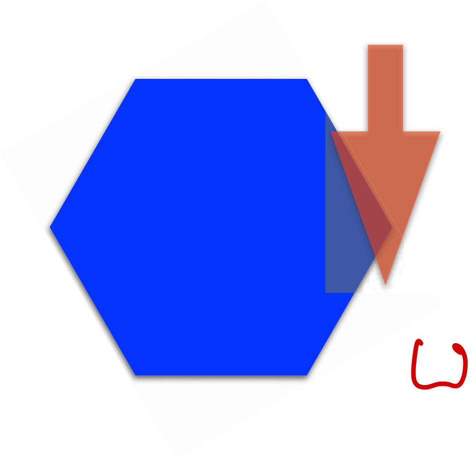

Wurtzite →

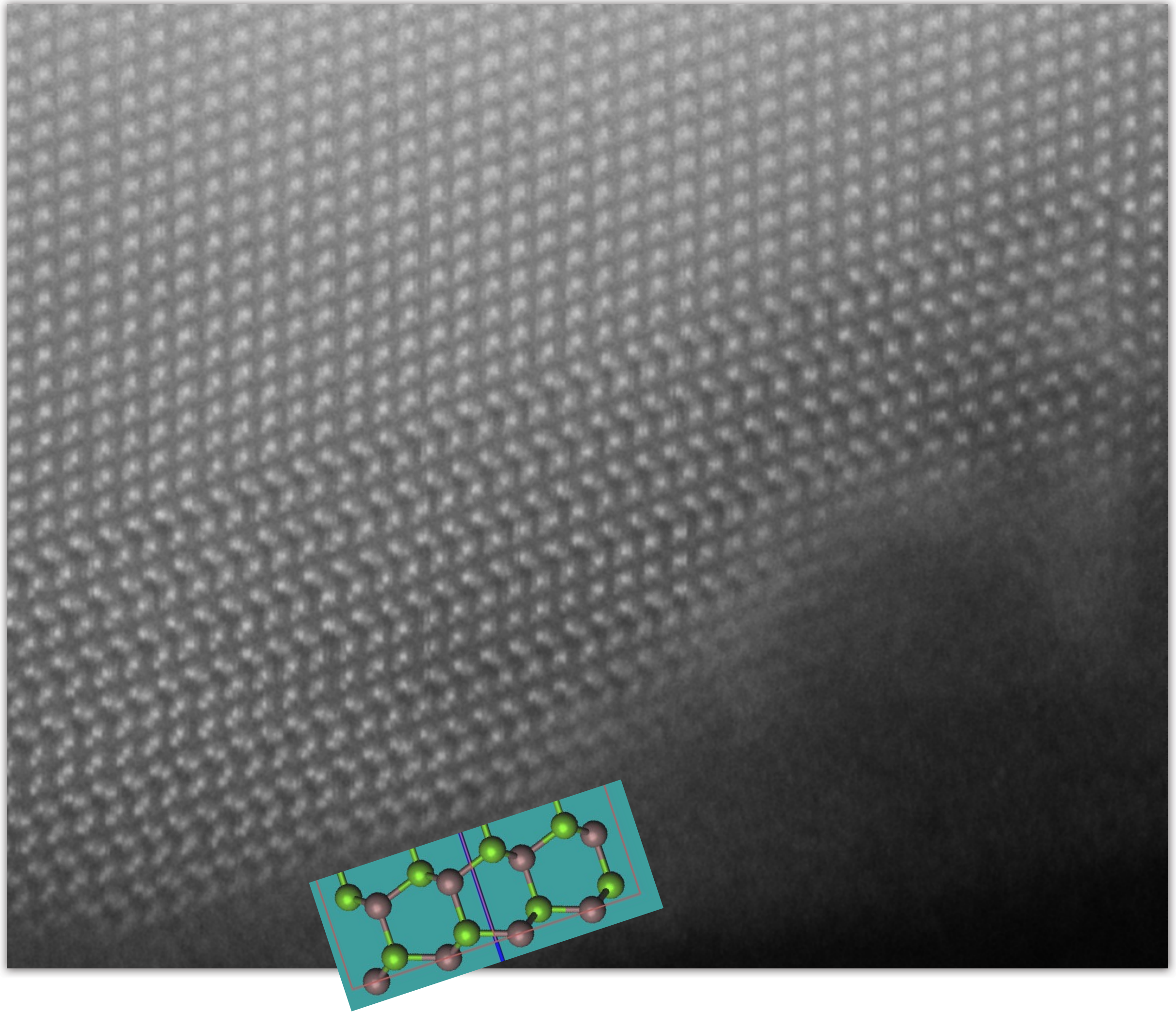

Sample courtesy of Yannick Fontana, Anna Fontcuberta-i-Morral, LMSC

Atomic resolution HAADF theory and simulation

Phonon scattering ↔ Mott scattering

- For scattering from *single atom*, Rez derived the phonon-scattering cross-section as:

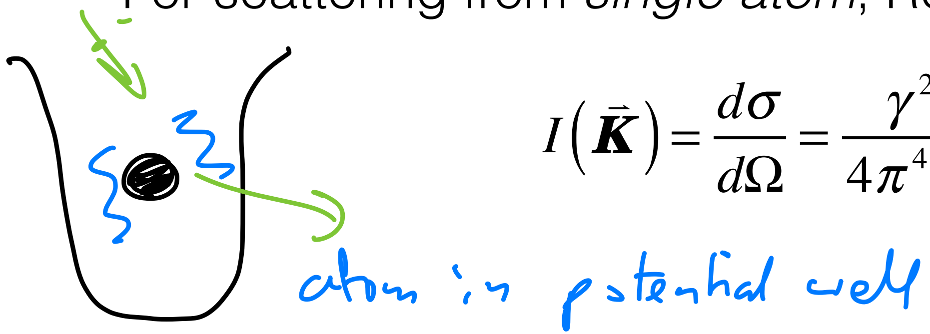

$$I(\vec{\boldsymbol{K}}) = \frac{d\sigma}{d\Omega} = \frac{\gamma^2}{4\pi^4 a_0^2} \frac{\left[Z - f_x(\vec{\boldsymbol{K}})\right]^2}{K^4} \left[1 - \exp\left(-\frac{MK^2}{2\pi^2}\right)\right]$$

- Plot of scattering cross-sections vs scattering angle (log scale for σ) ⟶
  - Short dashed line: Rutherford cross-section
  - Solid line: Mott scattering
  - Long dashed line: multiple-phonon scattering – often called "*thermal diffuse scattering*" (TDS)

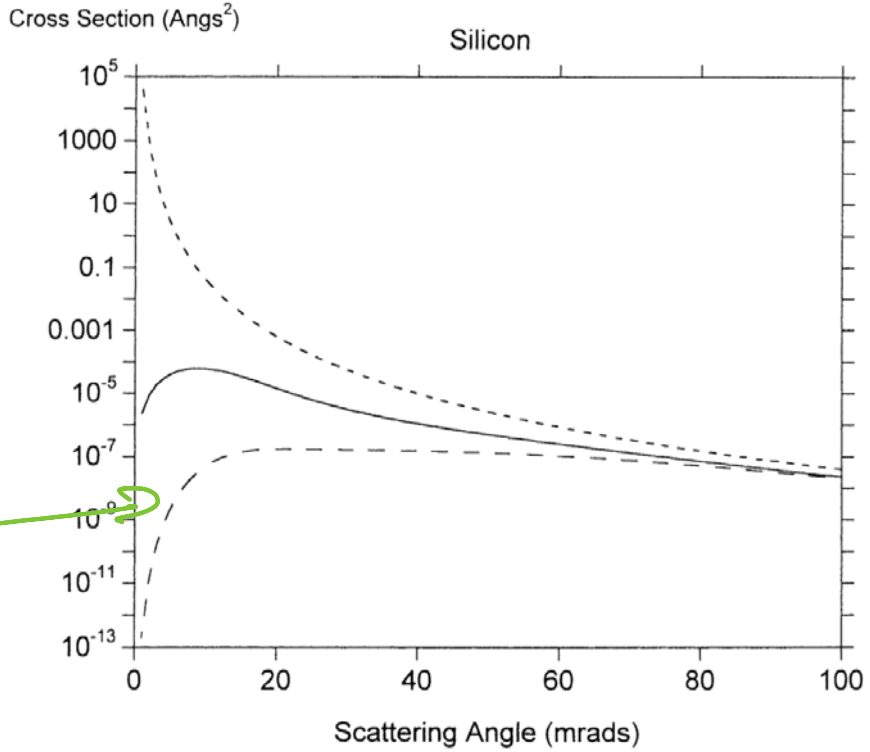

From: Rez Microsc. Microanal. **7** (2001) 356–362

Corrected probe depth of focus

- 3-dimensional calculations of probe shape show that it is only well focused over very limited depth of field
- Simulation for 300 keV beam, C_S = –149 nm
- However, for well-aligned atomic columns, electrons are focused by electric field of atoms, and beam *channels* down the column

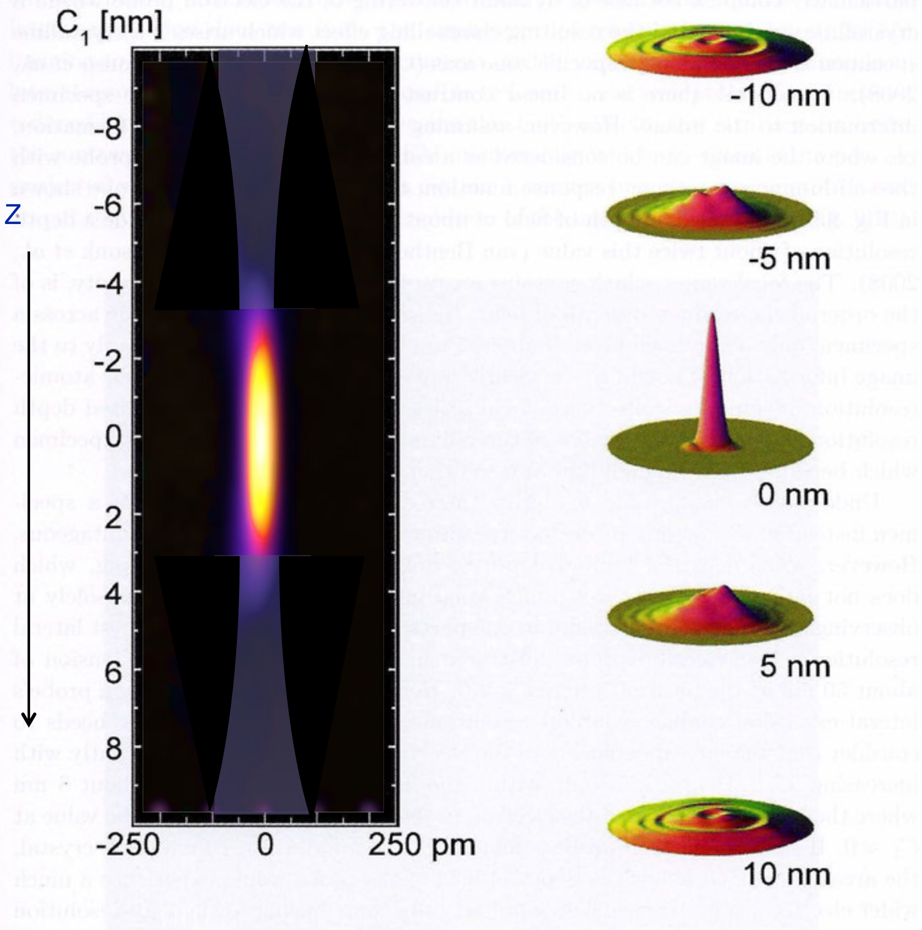

Fig. 9.9 Three-dimensional structure of a 300 keV electron probe formed with an illumination semi-angle of 29 mrad. The effective (Gaussian) source size is 25 pm and the residual geometrical aberrations considered in the probe calculation are A_2 = 24 nm, B_2 = 8 nm, C_3 = −149 nm, A_3 = 97 nm, S_3 = 90 nm, A_4 = 10.2 µm, D_4 = 7.2 µm, B_4 = 5.5 µ m, C_5 = 509 µm, A_5 = 221 µm, S_5 = 7 µm and R_5 = 24 µm. The energy length ℓ_C is 1.7 mm eV.

Small depth of field

Figure from: R. Erni, Aberration-Corrected Imaging in Transmission Electron Microscopy

Electron channeling

- When a (sub-)Å convergent probe focused on the top surface of a well aligned and spaced atomic column, the electron density is channeled down the column by the atomic nuclei
- This is often associated with a Bloch wave known as the 1*s* Bloch state, by analogy to 1*s* orbital of an atom
- At first approximation, high angle annular dark-field (HAADF) and annular bright field (ABF) images are consequence of the scattering of this 1*s*-state to their respective detectors
- HAADF image: channeling couples with thermal diffuse scattering

Phonon scattering

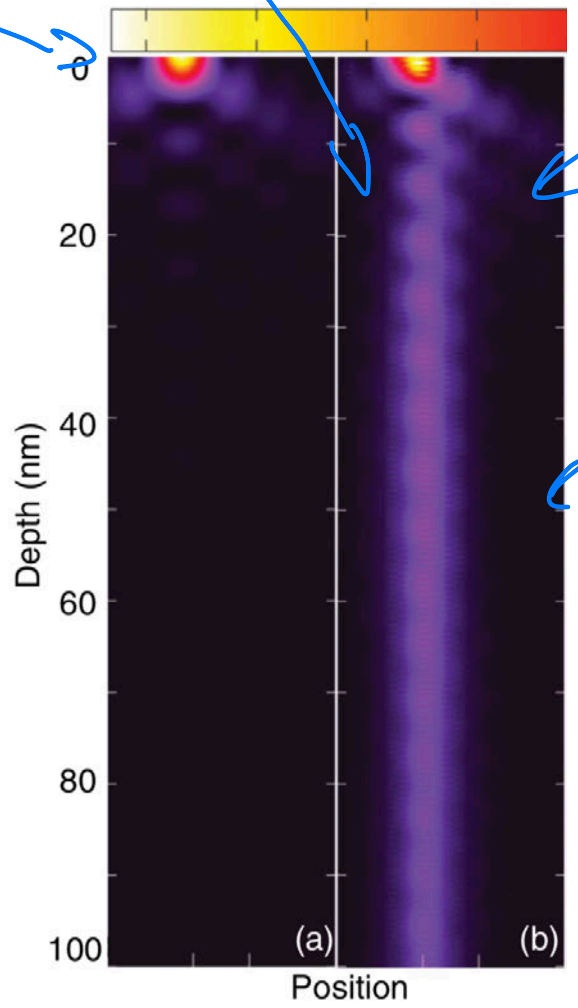

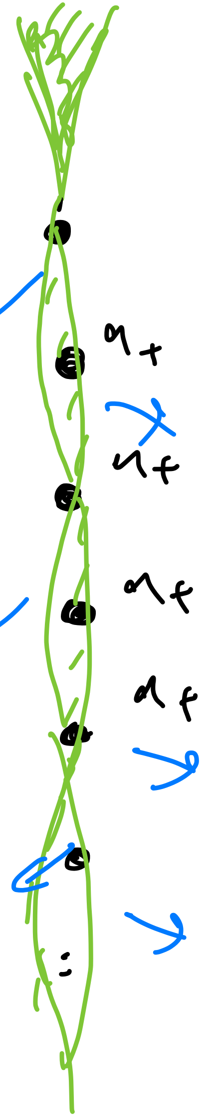

Figure from: Hovden et al. PRB **86** (2012) 195415

“Thermal diffuse scattering”

- “T*hermal diffuse scattering*” (TDS) is name given to incoherent scattering caused by thermal vibrations in the crystal lattice – i.e. phonons
- The small, random displacements of atoms/atomic nuclei caused by these vibrations are considered to scatter the electron beam/wave function incoherently
- This incoherent scattering, coupled to coherent elastic scattering, is responsible for formation of Kikuchi lines
- Conceptualised into a “frozen phonon” which is often used as the basis for a simulation methodology

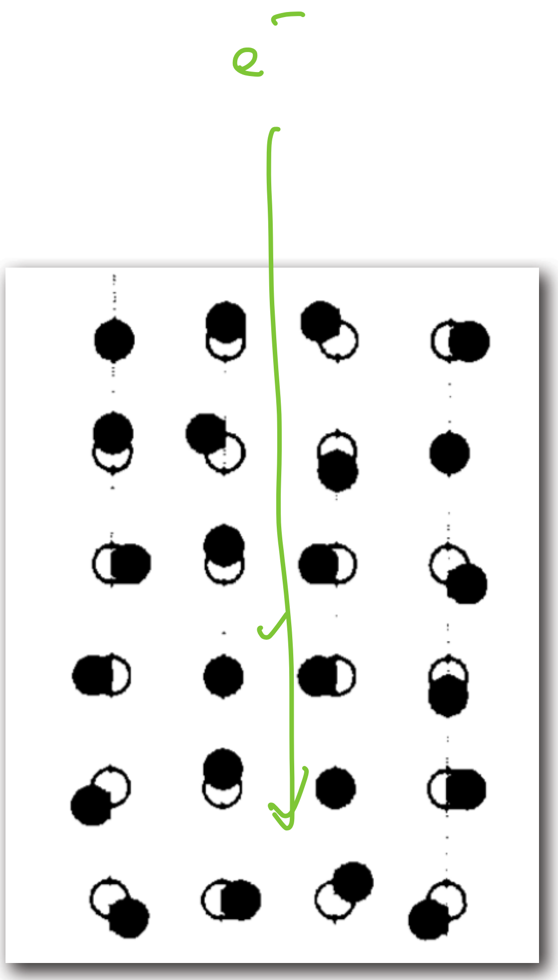

Loane and Silcox
Acta Cryst. A**47** (1991) 267–278

Atomic resolution HAADF theory

- Phonon scattering is an *inelastic* process. Transmitted electron suffers an energy loss of ~10–200 meV. Scattering nature is incoherent.
- Scattering involves the exchange of a phonon; e.g. the scattered e^- excites a phonon mode of a certain energy in the crystal lattice, and loses a corresponding amount of energy.
- Unlike plasmon and ionisation excitations (see coming lectures by C.H.), this scattering has high probability of giving a large momentum change to the transmitted e^-, scattering it to high angles
- Excitation of atomic nuclei – therefore strong scattering of 1*s*-state Bloch wave of e^- density channeling down the nuclei.
- HAADF detector collects these phonon-scattered electrons, allowing formation of image of atomic columns from this incoherent signal

Atomic resolution HAADF theory

- Inelastic nature of TDS/phonon scattering was experimentally confirmed by Hage et al.
- Using ultra high energy resolution electron energy-loss spectroscopy show that only the high angle scattered electrons which have 50–200 meV give the spatial intensity distribution of a HAADF image

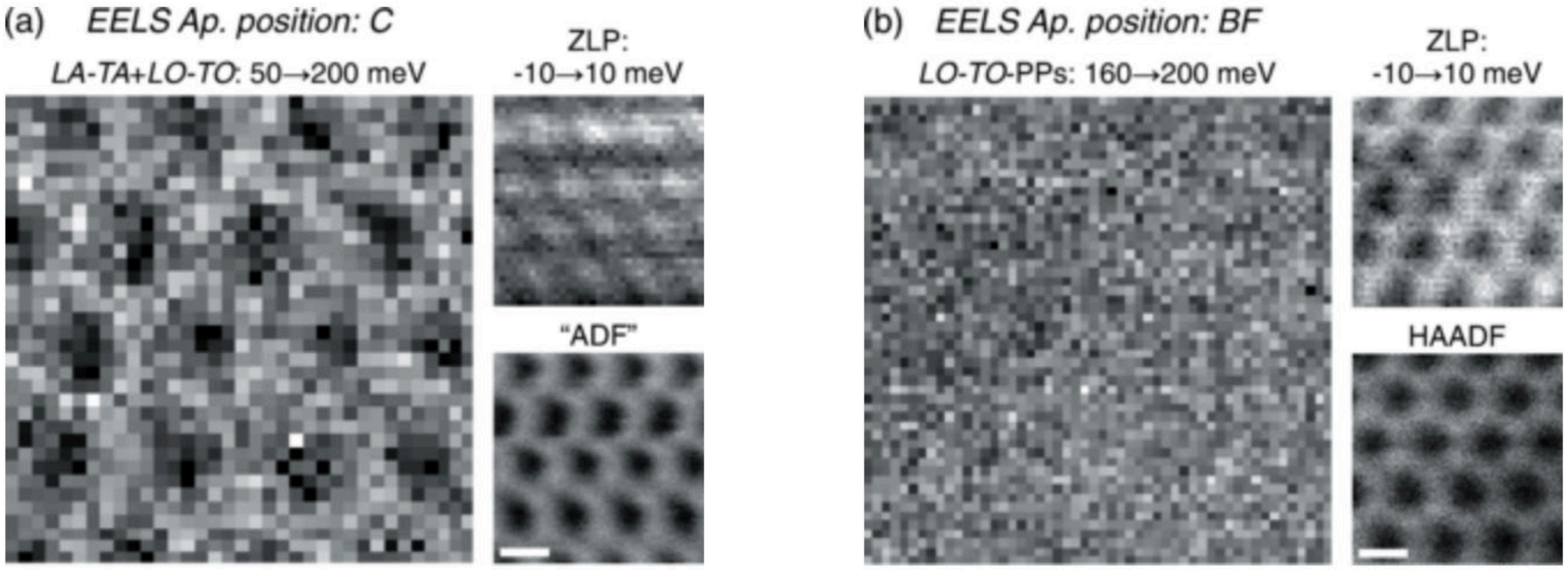

Hage et al., Phys. Rev. Lett. **122** (2019) 016103

Atomic resolution HAADF theory

- This inelastic, quantum mechanical exchange is incorporated into a simulation code based on a many-body quantum-mechanical model for phonon scattering introduced by Forbes et al. with Les Allen.
- Allows separation of incoherent, phonon-scattered intensity from coherent, elastically-scattered intensity.

CBED simulation

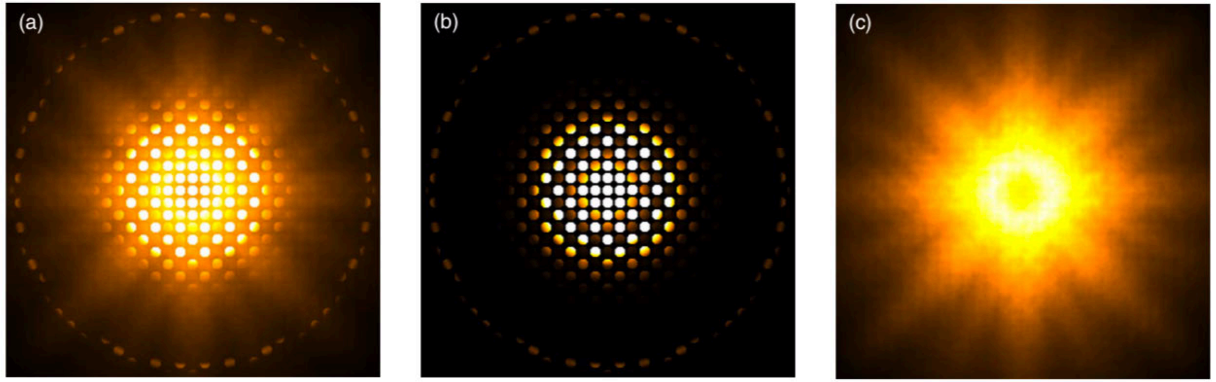

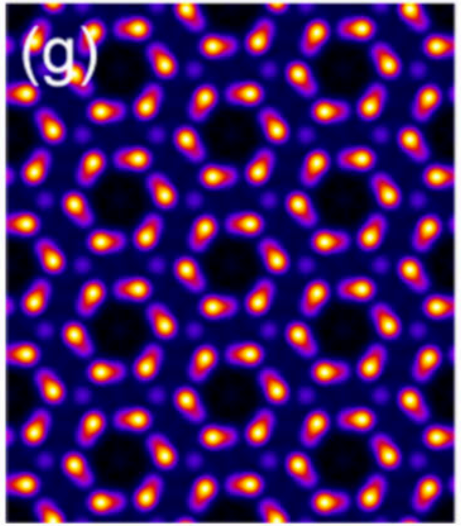

HAADF STEM simulation

Forbes et al., Phys. Rev. B **82** (2010) 104103; Les J. Allen et al. Ultramicroscopy **151** (2015) 11–22

Phase contrast STEM imaging for atomic resolution of light atoms

Atomic res^n HAADF : $I \propto Z^{1.6-1.9}$

If sample has heavy + light atoms

↳ Cannot image light atom columns

Annular bright-field (ABF)

- HAADF not useful for imaging light atoms in a sample with heavy atoms because contrast so strongly dependent on atomic number
- BF imaging has same disadvantages for imaging light atom columns as phase-contrast HR-TEM imaging
- Annular bright-field imaging (with aberration correction), where central part of BF detector is obscured, arguably solves these problems.
- For instance, for $\alpha = 22$ mrad, use $\beta = 11–22$ mrad.

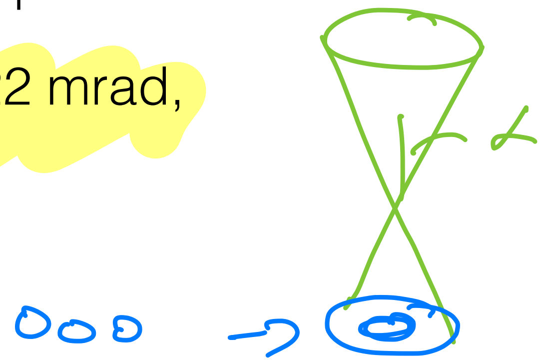

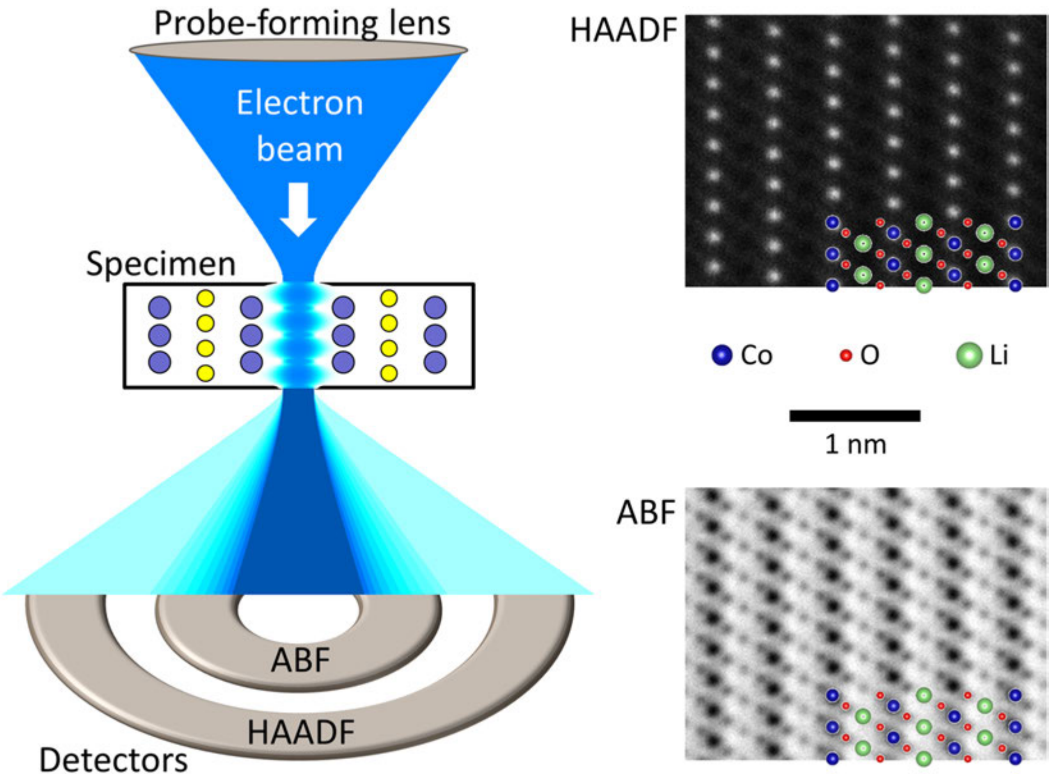

Li visualised in $LiCoO_2$ using ABF
Findlay et al. Microscopy **66** (2017) 3–14

Annular bright-field (ABF)

- Simulations show the ABF detector produces an “absorption” image in which light and heavy columns are visible and interpretable over a wide thickness range. Even H columns have been imaged.
- Optimal focal range very small (like HAADF) but slightly different optimum defocus to HAADF.

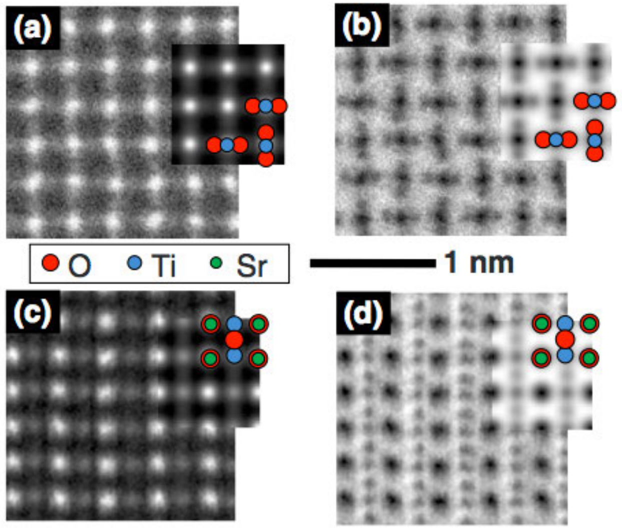

FIG. 1. (Color online) HAADF (left) and ABF (right) images (raw data) of (a) and (b) TiO_2 [001], and (c) and (d) $SrTiO_3$ [110]. Simulations and projected structures are given in the insets.

Findlay et al. APL **9**5 (2009) 191913

Annular bright-field (ABF)

- Simplified theory:
  - channeled e⁻ scattered mostly into centre of BF detector by light columns giving some dark ABF contrast (b)
  - e⁻ scattered more strongly to diffracted beams by heavy columns give darker ABF contrast (c)
  - between columns little scattering so brighter ABF contrast (a).

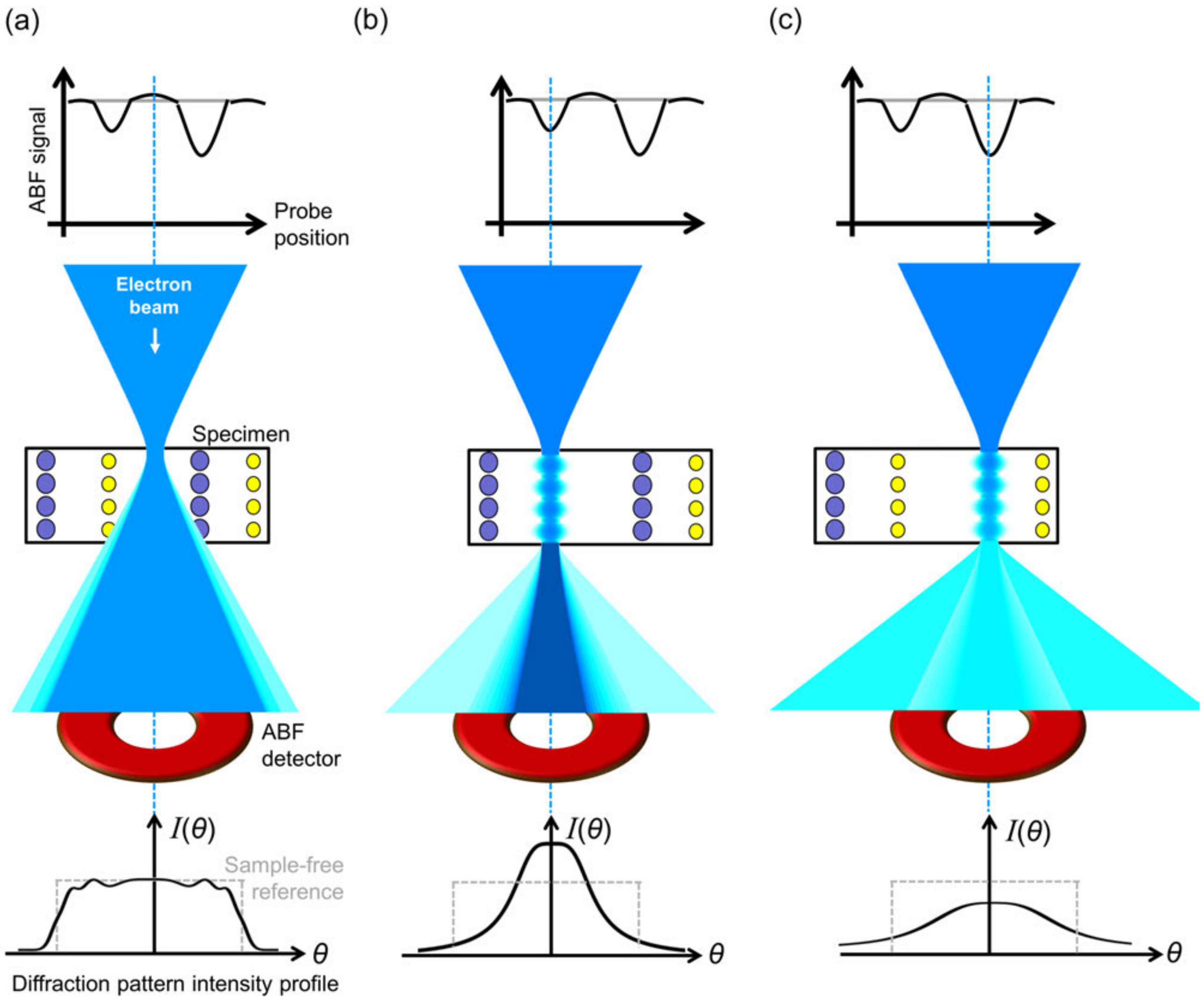

Findlay et al. Microscopy **66** (2017) 3–14

4D-STEM

- 2D grid detector records whole STEM CBED pattern (see last week's STEM intro)
- Also known as "pixelated STEM"
- Currently very active area of EM research, with new applications being developed
- Very rich (and large!) data sets, see this for some applications: https://www.youtube.com/watch?v=-KpxeNDoB5I

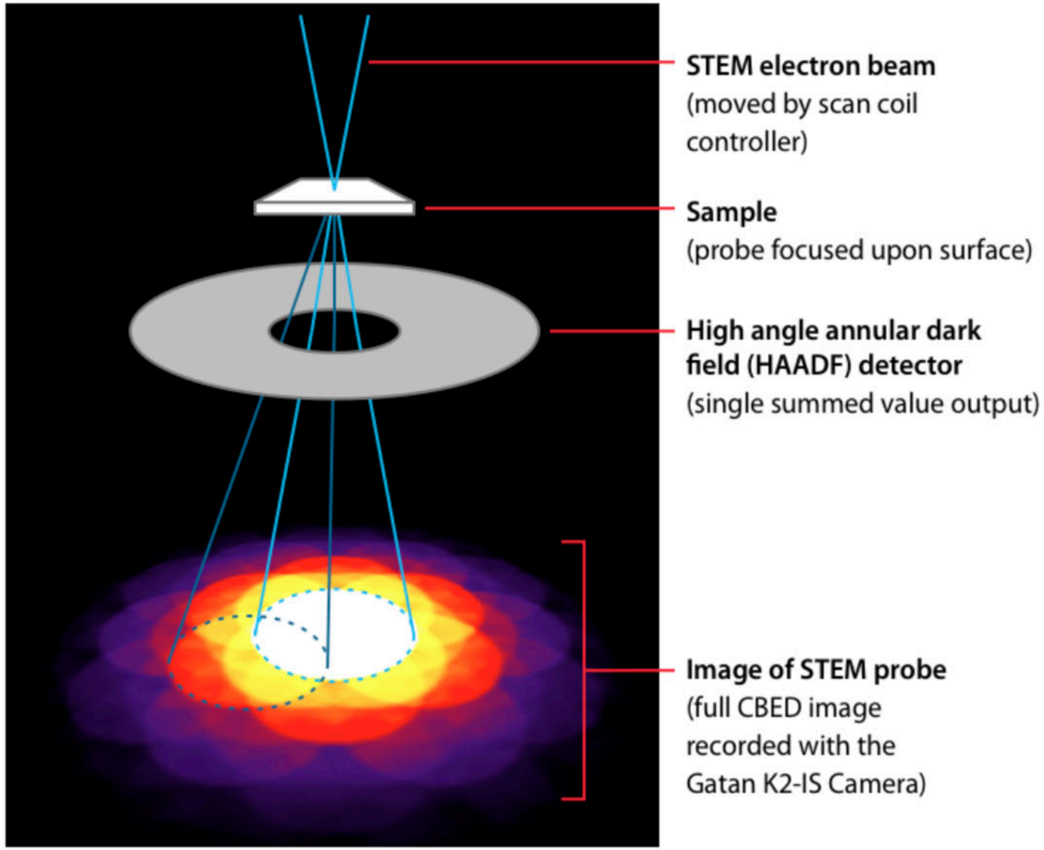

Schematic by Colin Ophus, Molecular Foundry

iCOM: integrated center of mass imaging

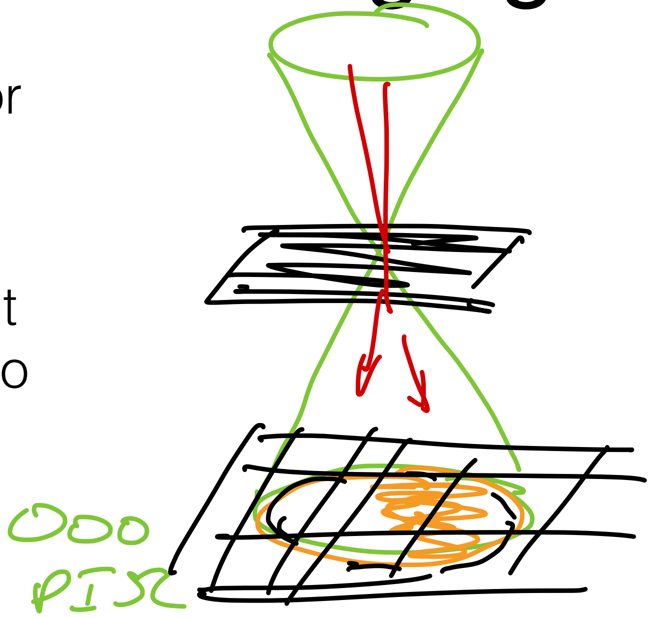

- Project STEM-CBED direct beam disc onto 4D-STEM detector
- As STEM probe moves, intensity distribution in disc varies
- In thin sample (i.e. weak phase approximation): displacement of center of mass (COM) of direct beam disc is proportional to gradient of phase shift of transmitted e⁻ wave →

  image intensity: $I^{(\mathrm{COM})}(\vec{r_p})$

- Taking integral of COM displacement vector gives phase shift and hence image intensity proportional to projected potential:

$$I^{(\mathrm{iCOM})}(\vec{r_p}) \propto V_t(\vec{r})$$

- Therefore should obtain atomic image with intensity proportional to atomic number *Z*

Lazic et al. Ultramicroscopy **160** (2016) 265

iDPC: integrated differential phase contrast

- Like iCOM but use a simpler and faster detector
- Project direct beam disc on 4 quadrant segmented detector, calculate iDPC
- DPC: differential phase contrast: image intensity of one quadrant minus opposite quadrant (C - A) (D - B)
- Still can work well for imaging light and heavy atoms when sample is much thicker than weak phase object

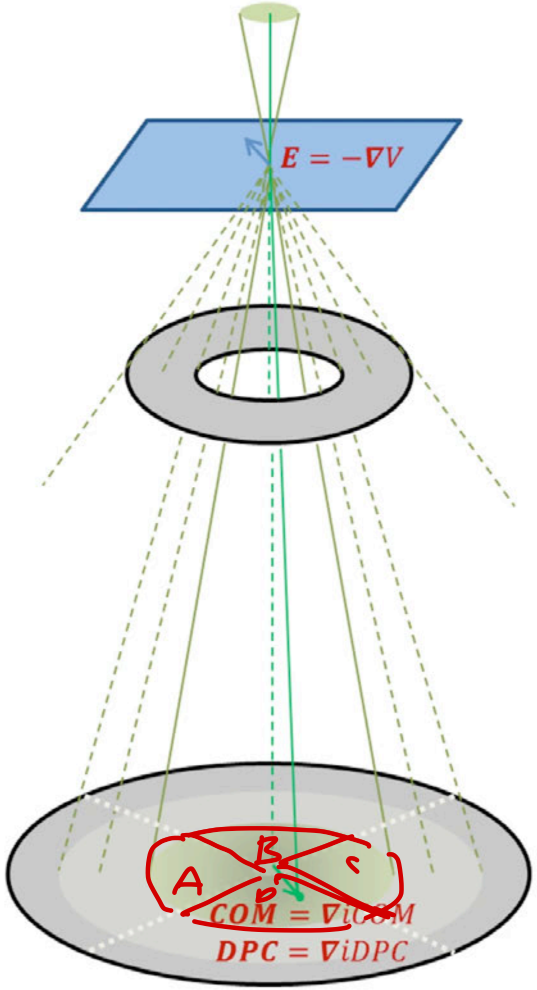

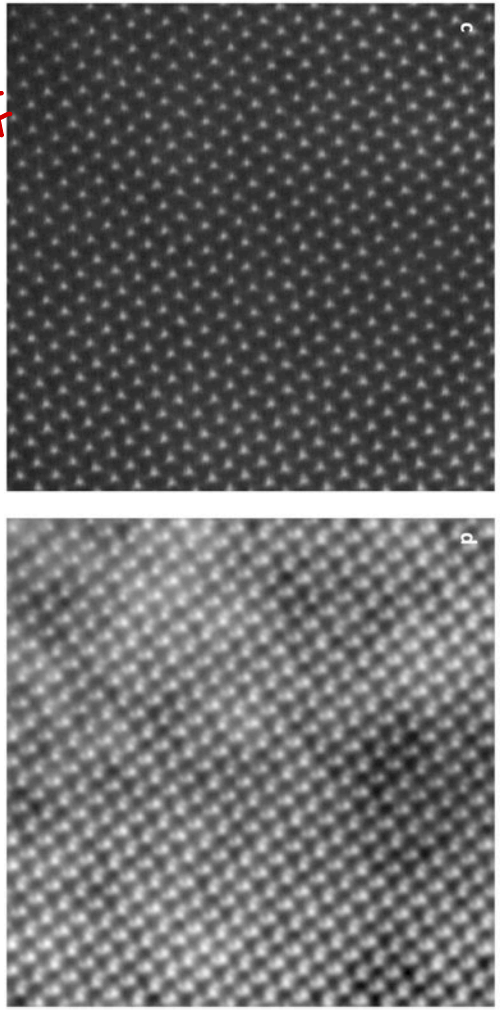

Electron ptychography (single slice)

- *Ptychography*: uses 4D STEM data to retrieve phase differences from interference patterns of overlapped diffracted beams
  ⟹ Go beyond diffraction limit for “super resolution”!

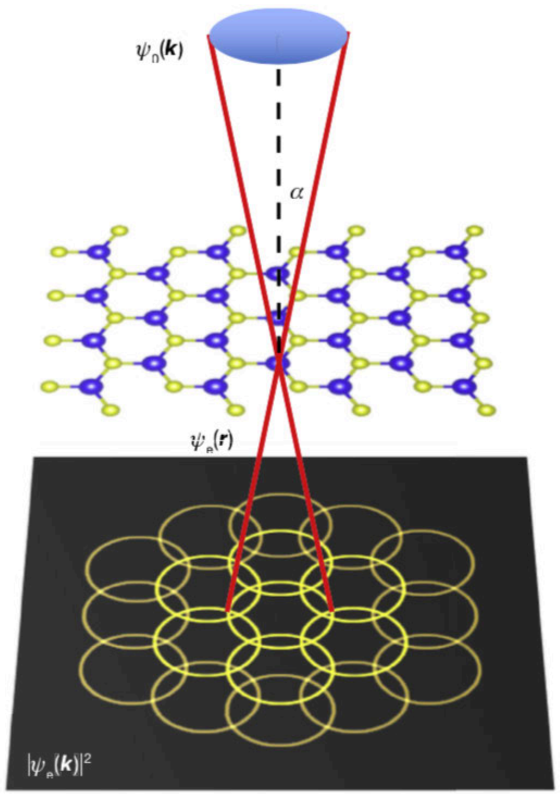

Imaging monolayer MoS_2

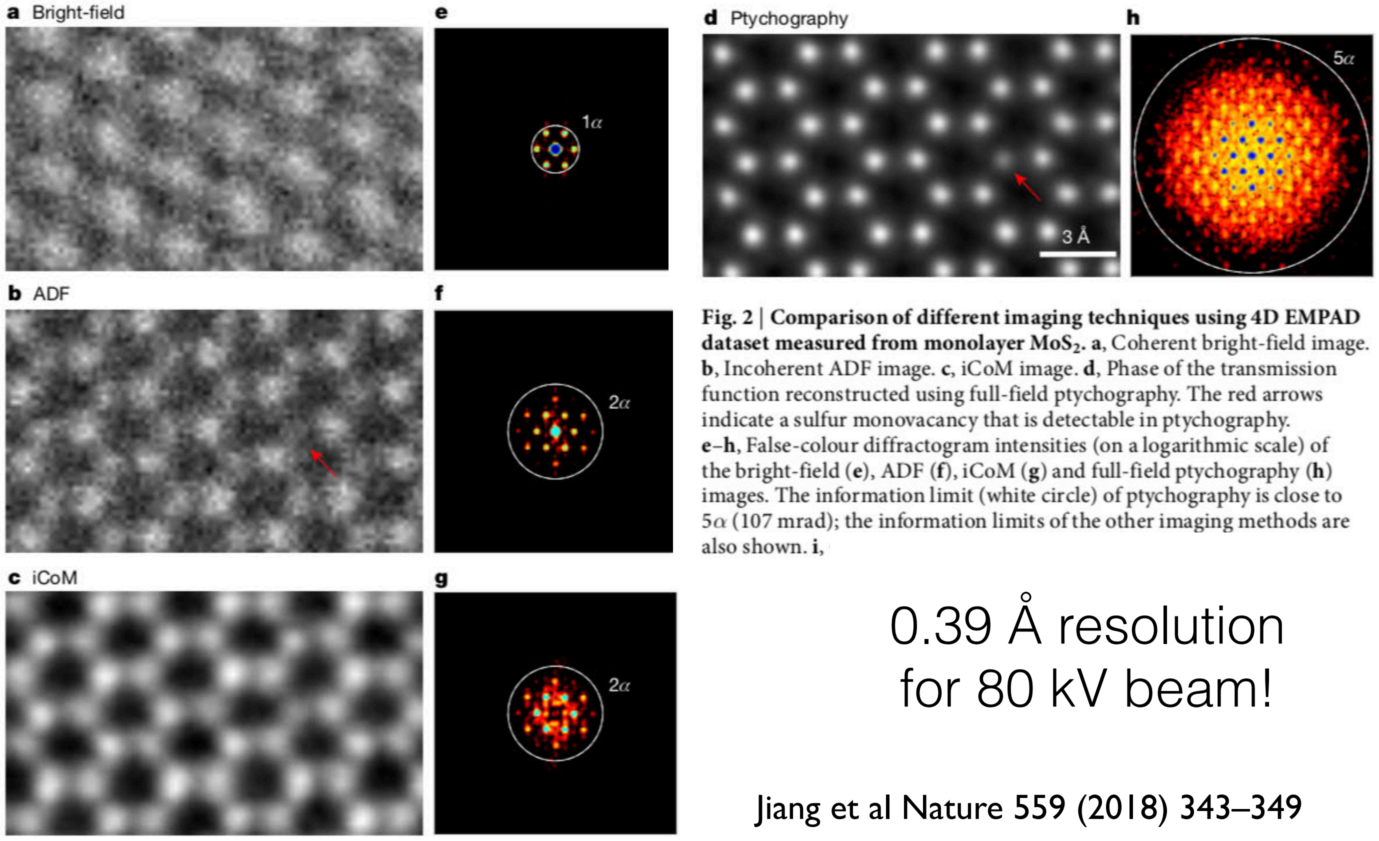

Fig. 2 | Comparison of different imaging techniques using 4D EMPAD dataset measured from monolayer MoS_2. a, Coherent bright-field image. **b,** Incoherent ADF image. **c,** iCoM image. **d,** Phase of the transmission function reconstructed using full-field ptychography. The red arrows indicate a sulfur monovacancy that is detectable in ptychography. **e–h,** False-colour diffractogram intensities (on a logarithmic scale) of the bright-field (**e**), ADF (**f**), iCoM (**g**) and full-field ptychography (**h**) images. The information limit (white circle) of ptychography is close to 5α (107 mrad); the information limits of the other imaging methods are also shown. **i,**

0.39 Å resolution
for 80 kV beam!

Jiang et al Nature 559 (2018) 343–349

Electron ptychography (multislice)

- “Inverse” multislice ptychographic reconstruction for “thick” samples (15–30 nm)
- $PrScO_3$ on [001] with 59 pm spaced Pr dumbbells:

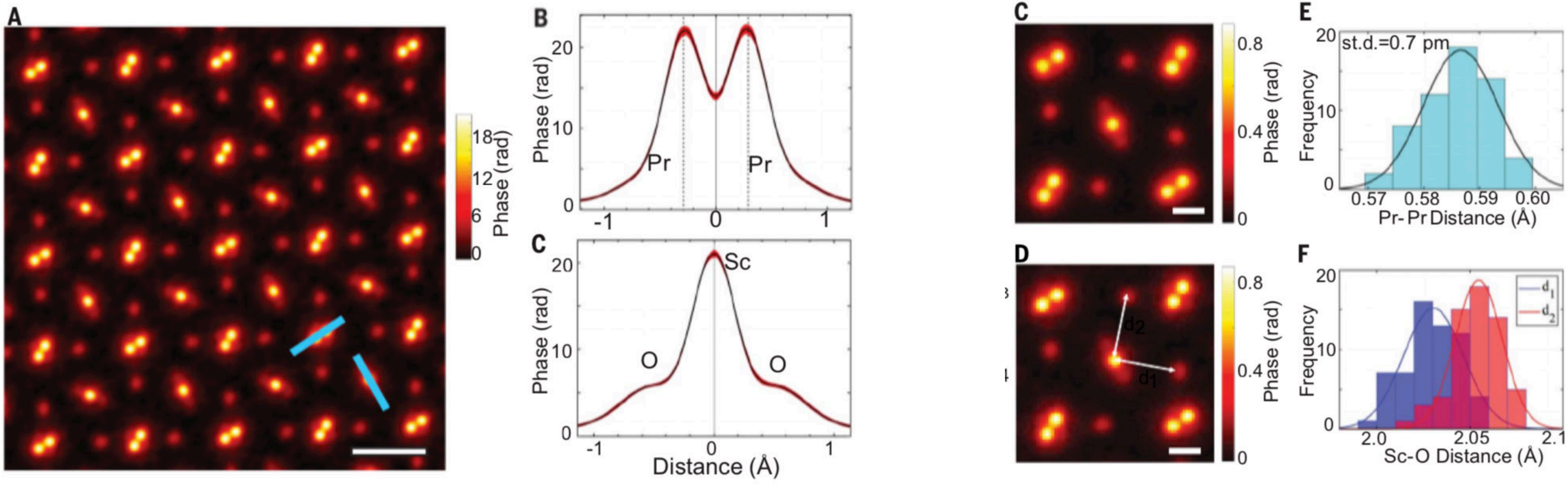

- “The measured widths of atomic columns are limited by thermal fluctuations of the atoms” – instrumental blurring of < 20 pm!

Chen et al. Science **372** (2021) 826